NONRECIPROCAL MICROWAVE DEVICES USING PARAMETRIC FREQUENCY CONVERSION

BY

JOHN A. KROL

THESIS

Submitted in partial fulfillment of the requirements
for the degree of Master of Science in Electrical and Computer Engineering
in the Graduate College of the
University of Illinois at Urbana-Champaign, 2017

Urbana, Illinois

Adviser:

Assistant Professor Songbin Gong

ABSTRACT

This thesis endeavors to characterize the performance of nonreciprocal microwave devices enabled by parametric frequency conversion. Although such devices have been explored somewhat superficially in the 1960s, resurgent interest in low-noise nonreciprocal components has motivated new research in parametric frequency conversion. In particular, this work explores the contributions of nonidealities to performance degradation of a parametric gyrator. Expressions are developed for loss and noise performance contributed by nonideal components constituting the gyrator, and simulations are used to verify the findings. The gyrator is then used to construct a circulator, and its performance's dependence on the same nonidealities is evaluated. A simulated design example is used to demonstrate a practical realization of such a circulator.

"Du Sterne hellster, o wie schön verkündest du den Tag! Wie schmückst du ihn, o Sonne du, des Weltalls Seel' und Aug'! Ihr' Elemente, deren Kraft, stets neue Formen zeugt..."

-Gottfried van Swieten

From the libretto to Haydn's "Die Schöpfung"

ACKNOWLEDGMENTS

The author wishes to express gratitude to Dr. Gong for his tireless efforts in shaping this thesis into a respectable document. Special thanks also to Dr. Pete Dragic for encouraging me to pursue my master's degree and for introducing me to the world of academic research. Thanks also to my family, especially my mother, Judy, and my father, Steve, who both taught me the value of hard work and encouraged my studies at every moment. Thanks also to my uncle Dan, who first sparked my interest in electrical engineering. Finally, thanks to my girlfriend, Peng, whose unmatched skill at the piano has filled my life with the sounds of Schumann, Brahms and Beethoven.

TABLE OF CONTENTS

LIST OF FIGURES

LIST OF SYMBOLS

Y_{ij}	Admittance Parameter for Ports i and j
ω	Angular Frequency ($\omega = 2\pi f$)
G_A	Available Gain
I	Current
C_1	Dynamic Capacitance at Frequency f_{LO}
ξ	Dynamic Loss Factor
Q_{d}	Dynamic Quality Factor
$\bar{\bar{\sigma}}$	Electric Conductivity Tensor
$\vec{J}$	Electric Current Density
$\vec{E}$	Electric Field Intensity
$\bar{\bar{\epsilon}}$	Electric Permittivity Tensor
Z_{ij}	Impedance Parameter for Ports i and j
IL	Insertion Loss
ω_{IF}	Intermediate Angular Frequency ($\omega = 2\pi f_{\mathrm{IF}}$)
ω_-	Inverting Converted Angular Frequency ($\omega = 2\pi f_-$)
f	Linear Frequency
ω_{LO}	Local Oscillator Angular Frequency ($\omega = 2\pi f_{\mathrm{LO}}$)
$\vec{M}$	Magnetic Current Density
$\vec{H}$	Magnetic Field Intensity
$\bar{\bar{\mu}}$	Magnetic Permeability Tensor
ψ	Modulation Parameter
F	Noise Factor

NF	Noise Figure ($NF = 10 \log F$)
ω_+	Non-inverting Converted Angular Frequency ($\omega = 2\pi f_+$)
W	Power ($W = VI^*$)
G_P	Power Gain
S_{ij}	Scattering Parameter for Ports i and j
R_c	Series Loss Resistance
SNR	Signal-to-Noise Ratio
C_0	Static Capacitance
G_T	Transducer Gain
V	Voltage
e	Waveguide Modal Electric Field Distribution
h	Waveguide Modal Magnetic Field Distribution

CHAPTER 1

INTRODUCTION

Electrical circuits with variable parameters are known as *parametric circuits*. Most often, the term is used to describe circuits containing a lossless element with a parameter that varies in time. One example of this would be the variation of the reverse-bias capacitance of an ideal varactor diode by an external voltage source. In such a circuit, an excitation of one frequency can be used to generate signals of many other frequencies. Although the concept of parametric excitation was first observed in a mechanical system by Michael Faraday [1] in 1831, it was first applied to electrical circuits in 1892 by G. F. FitzGerald [2]. Throughout the 20th century, parametric circuits were utilized often in high-sensitivity receiver systems for satellite communications [3, 4, 5] or as amplifiers in radar systems [6, 7, 8] due to their unique low-noise properties and their ability to operate at microwave frequencies. Before the invention of the high electron mobility transistor (HEMT) [9], parametric amplifiers built with varactor diodes were the only solid-state technique to amplify a signal at microwave frequencies. Although parametric circuits fell largely into obscurity with the invention of the HEMT, they have found new applications in modern times as the demand has grown for small, low-noise nonreciprocal microwave elements readily realized in integrated form. This demand comes largely from the communications industry, where such components are needed to achieve full-duplex communication, also called *simultaneous transmit-and-receive* (STAR). In this scheme, a transceiver can transmit and receive information at the same time and the same frequency. This is in contrast to time domain duplex, where transmission and reception are performed at different times, or frequency domain duplex, where each is done at different frequencies. Intuitively, STAR could be used to double the bandwidth of conventional transceivers.

1.1 Reciprocity and Noise in Microwave Devices

The behavior of signals traveling in different directions inside a microwave device is known as the *reciprocity* of the device. When discussing the reciprocity of the device, it is convenient to describe the device as an n-port network, where a port is a pair of terminals. In this case, the formalism of scattering parameters can be used to classify the device. For a *reciprocal device*, the scattering parameters must satisfy the relation shown in equation 1.1.

$$S_{ij} = S_{ji}, \quad i \neq j, \quad i = 1, 2, 3...n, \quad j = 1, 2, 3...n \tag{1.1}$$

This means that if some voltage V_a is applied at some port i and a corresponding voltage V_b is measured at port j, then the same voltage V_b should be measured at port i if V_a is applied to port j. For a *nonreciprocal device*, relation in equation 1.1 is not satisfied for at least one pair of ports. This means that for at least one pair of ports i and j, if some voltage V_a is applied to port i and V_b is measured at port j, it will be observed that some voltage $V_c \neq V_b$ is measured at port i if V_a is now applied to port j. The existence of these two types of devices can be demonstrated from Maxwell's equations using the *reciprocity theorem* [10].

1.1.1 Reciprocity Theorem and Relation to Electrical Circuits

In the study of electromagnetic fields and waves, there exists an important theorem relating the behavior of two independent fields generated by two independent sources. This theorem originates from the fact that both fields are governed by Maxwell's equations and is known as the *reciprocity theorem*. Although the theorem exists in several forms and can be generalized to an arbitrary number of independent sources, the form known as the *Lorentz reciprocity theorem* is most amenable to the description of circuits. The theorem can be derived by first considering two independent electromagnetic fields: $(\vec{E}_1, \vec{H}_1)$ and $(\vec{E}_2, \vec{H}_2)$. Each of these field quantities is a vector in

three-dimensional space, and thus can be represented with a column vector. In the context of an electrical circuit, such as a two-port device, these independent fields could represent a signal incident upon port one and a signal incident upon port two. These fields follow Ampère's and Faraday's laws, meaning

$$\nabla \times \vec{E_1} = -j\omega\bar{\bar{\mu}}\vec{H_1} - \vec{M_1} \tag{1.2}$$

$$\nabla \times \vec{H_1} = (j\omega\bar{\bar{\epsilon}} + \bar{\bar{\sigma}})\vec{E_1} + \vec{J_2} \tag{1.3}$$

$$\nabla \times \vec{E_2} = -j\omega\bar{\bar{\mu}}\vec{H_2} - \vec{M_2} \tag{1.4}$$

$$\nabla \times \vec{H_2} = (j\omega\bar{\bar{\epsilon}} + \bar{\bar{\sigma}})\vec{E_2} + \vec{J_2} \tag{1.5}$$

In the most general case, the material parameters $\bar{\bar{\mu}}$, $\bar{\bar{\epsilon}}$ and $\bar{\bar{\sigma}}$ are expressed as tensors with positional dependence. In rectangular coordinates,

$$\epsilon(x,y,z) = \begin{pmatrix} \epsilon_{xx}(x,y,z) & \epsilon_{xy}(x,y,z) & \epsilon_{xz}(x,y,z) \\ \epsilon_{yx}(x,y,z) & \epsilon_{yy}(x,y,z) & \epsilon_{yz}(x,y,z) \\ \epsilon_{zx}(x,y,z) & \epsilon_{zy}(x,y,z) & \epsilon_{zz}(x,y,z) \end{pmatrix}$$

$$\mu(x,y,z) = \begin{pmatrix} \mu_{xx}(x,y,z) & \mu_{xy}(x,y,z) & \mu_{xz}(x,y,z) \\ \mu_{yx}(x,y,z) & \mu_{yy}(x,y,z) & \mu_{yz}(x,y,z) \\ \mu_{zx}(x,y,z) & \mu_{zy}(x,y,z) & \mu_{zz}(x,y,z) \end{pmatrix}$$

$$\sigma(x,y,z) = \begin{pmatrix} \sigma_{xx}(x,y,z) & \sigma_{xy}(x,y,z) & \sigma_{xz}(x,y,z) \\ \sigma_{yx}(x,y,z) & \sigma_{yy}(x,y,z) & \sigma_{yz}(x,y,z) \\ \sigma_{zx}(x,y,z) & \sigma_{zy}(x,y,z) & \sigma_{zz}(x,y,z) \end{pmatrix}$$

The physical reason for this is that, in general, material parameters can be dependent on the direction of propagation of EM waves. This is referred to as *anisotropy*. If these material parameters are spatially dependent, this is referred to as *inhomogeneity*. Rearranging equations 1.2, 1.3, 1.4 and 1.5 yields

$$\nabla\cdot(\vec{H_2}\times\vec{E_1}) = -j\omega\bar{\bar{\epsilon}}\vec{E_1}\cdot\vec{E_2} + \bar{\bar{\sigma}}\vec{E_1}\cdot\vec{E_2} + j\omega\bar{\bar{\mu}}\vec{H_2}\cdot\vec{H_1} + \vec{E_1}\cdot\vec{J_2} + \vec{H_2}\cdot\vec{M_1} \tag{1.6}$$

$$\nabla\cdot(\vec{H_1}\times\vec{E_2}) = -j\omega\bar{\bar{\epsilon}}\vec{E_2}\cdot\vec{E_1} + \bar{\bar{\sigma}}\vec{E_2}\cdot\vec{E_1} + j\omega\bar{\bar{\mu}}\vec{H_1}\cdot\vec{H_2} + \vec{E_2}\cdot\vec{J_1} + \vec{H_1}\cdot\vec{M_2} \tag{1.7}$$

For a symmetric tensor, its product with a vector is commutative, which is to say $\bar{\bar{\alpha}}\vec{A} = \vec{A}\bar{\bar{\alpha}}$, and thus if $\bar{\bar{\mu}}$, $\bar{\bar{\epsilon}}$ and $\bar{\bar{\sigma}}$ are all symmetric, then subtracting equation 1.7 from 1.6 yields

$$\nabla \cdot (\vec{H}_2 \times \vec{E}_1 - \vec{H}_1 \times \vec{E}_2) = \vec{E}_1 \cdot \vec{J}_2 + \vec{H}_2 \cdot \vec{M}_1 - \vec{E}_2 \cdot \vec{J}_1 - \vec{H}_1 \cdot \vec{M}_2 \quad (1.8)$$

Materials that satisfy this condition are known as *reciprocal materials*. If equation 1.8 is integrated over a region of finite volume V that contains no sources (i.e. $\vec{J}_i = 0, \vec{M}_i = 0$), then applying the divergence theorem yields 1.9

$$\oiint_S (\vec{E}_1 \times \vec{H}_2) \cdot \hat{n}\, dS = \oiint_S (\vec{E}_2 \times \vec{H}_1) \cdot \hat{n}\, dS \quad (1.9)$$

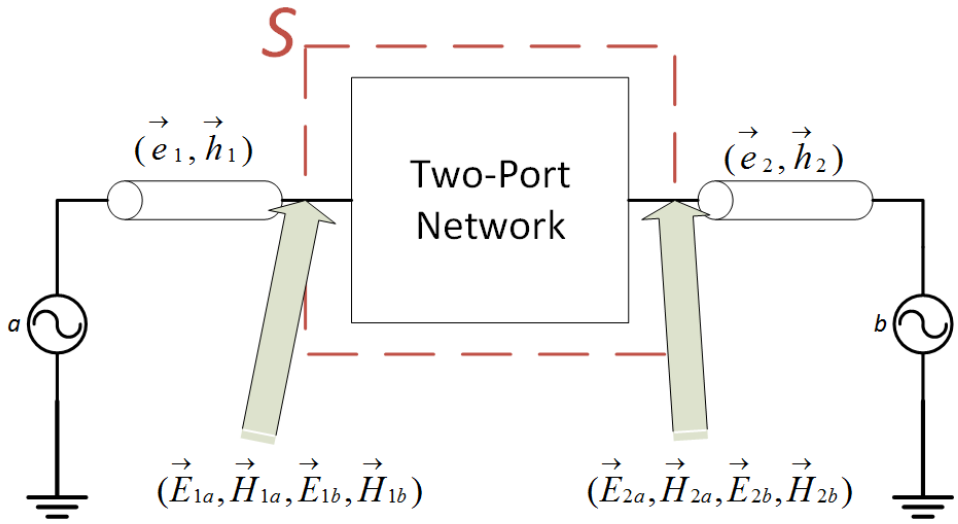

Figure 1.1: Two-port network. Ports 1 and 2 are driven by sources a and b, respectively. Each source is connected to the two-port via a waveguide with modal fields shown. Surface S encloses the two-port.

This is the Lorentz reciprocity theorem. Per the definition of the divergence theorem, S is the closed surface that encloses V, and $\hat{n}$ is the unit vector normal to S. Now, consider a two-port network with sources a and b driving ports 1 and 2, respectively, as shown in Fig. 1.1. The surface S is now defined to enclose the boundaries of the network. Each port is a pair of terminals,

and can be addressed by some type of waveguide. If the waveguides are constructed from perfect electrical conductors, the fields excited in each due to some source can be expressed in terms of each waveguide's transverse modal fields. If the waveguide connecting port 1 has modal fields ($\vec{e}_1$, $\vec{h}_1$) and the waveguide at port 2 has modal fields ($\vec{e}_2$, $\vec{h}_2$), then the fields at each port due to each source can be linearly related to the modal fields as shown in 1.10.

$$\vec{E}_{1a} = V_{1a}\vec{e}_1, \quad \vec{H}_{1a} = I_{1a}\vec{h}_1 \tag{1.10a}$$
$$\vec{E}_{1b} = V_{1b}\vec{e}_1, \quad \vec{H}_{1b} = I_{1b}\vec{h}_1 \tag{1.10b}$$
$$\vec{E}_{2a} = V_{2a}\vec{e}_2, \quad \vec{H}_{2a} = I_{2a}\vec{h}_2 \tag{1.10c}$$
$$\vec{E}_{1b} = V_{2b}\vec{e}_2, \quad \vec{H}_{2b} = I_{2b}\vec{h}_2 \tag{1.10d}$$

Each field is denoted with a two-part subscript with the first part being the port and the second being the source. For example, $\vec{E}_{1a}$ is the electric field at port 1 excited by source a. Now, 1.10 can be substituted into 1.9 to obtain

$$(V_{1a}I_{1b} - V_{1b}I_{1a}) \oiint_S (\vec{e}_1 \times \vec{h}_1) \cdot \hat{n}\, dS + (V_{2a}I_{2b} - V_{2b}I_{2a}) \oiint_S (\vec{e}_2 \times \vec{h}_2) \cdot \hat{n}\, dS = 0 \tag{1.11}$$

Comparing equations 1.10 and 1.9, then it can be seen that

$$\oiint_S (\vec{e}_1 \times \vec{h}_1) \cdot \hat{n}\, dS = \oiint_S (\vec{e}_2 \times \vec{h}_2) \cdot \hat{n}\, dS = 1 \tag{1.12}$$

and now equation 1.11 can be reduced to

$$(V_{1a}I_{1b} - V_{1b}I_{1a}) + (V_{2a}I_{2b} - V_{2b}I_{2a}) = 0 \tag{1.13}$$

Next, one must consider the definition of the admittance matrix:

$$\begin{bmatrix} I_1 \\ I_2 \end{bmatrix} = \begin{pmatrix} Y_{11} & Y_{12} \\ Y_{21} & Y_{22} \end{pmatrix} \begin{bmatrix} V_1 \\ V_2 \end{bmatrix} \tag{1.14}$$

Using this definition, equation 1.13 can be rewritten as

$$(V_{1a}V_{2b} - V_{1b}V_{2a})(Y_{12} - Y_{21}) = 0 \tag{1.15}$$

Since sources a and b are independent, the total voltage at each port due to each source can take on arbitrary values, and the only way to satisfy equation 1.15 is to have $Y_{21} = Y_{12}$. Although this is a proof for the admittance matrix, the effect of reciprocity on the scattering matrix of this network can be demonstrated without going into the definition of the scattering matrix itself. It has been demonstrated that the relationship between Y and S is

$$S_{12} = \frac{-2Z_0Y_{12}}{\Delta} \tag{1.16a}$$

$$S_{21} = \frac{-2Z_0Y_{21}}{\Delta} \tag{1.16b}$$

with Δ as the determinant of the admittance matrix. Since $Y_{12} = Y_{21}$, it is clear that $S_{12} = S_{21}$. The theorem of equation 1.9 can be generalized to an arbitrary number of fields, meaning a reciprocal n-port network will have, for $i = 1, 2, 3...n$, $j = 1, 2, 3...n$ and $i \neq j$, $S_{ij} = S_{ji}$. As stated earlier, an n-port network constructed with reciprocal materials follows this requirement. In this work, it will be shown that networks with lossless, time-varying elements can violate this theorem.

1.1.2 Nonreciprocal Devices

In microwave engineering, some designs require components that manipulate signals differently depending on their direction of propagation [10]. As stated before, reciprocal devices have $S_{ij} = S_{ji}$, and therefore cannot perform these tasks. Instead, nonreciprocal devices are required. This section

describes three common devices to familiarize the reader with the utility of nonreciprocal components.

1.1.2.1 Circulators

A circulator is a device that transmits signals from one port to the next in a successive rotation , but blocks transmission in the opposite rotation. It is also matched at all ports. Although a circulator can have $n > 2$ ports, three-port and four-port circulators are the most common. The *handedness* of a circulator is the rotation direction of circulation. A right-handed three-port circulator circulates power in a succession of ports as $1 \rightarrow 2 \rightarrow 3 \rightarrow 1$. Its scattering matrix is

$$S = \begin{pmatrix} 0 & 1 & 0 \\ 0 & 0 & 1 \\ 1 & 0 & 0 \end{pmatrix} \tag{1.17}$$

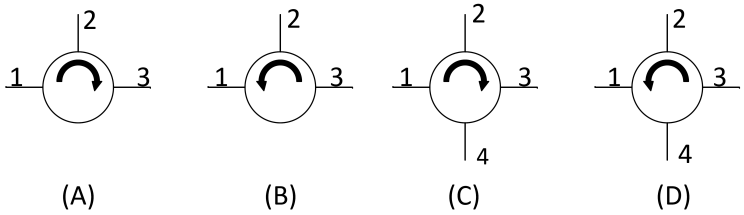

Figure 1.2: System-level representation of various circulators. The curved arrows represent the sense of rotation.

A left-handed three-port circulator circulates power in a succession of ports as $1 \rightarrow 3 \rightarrow 2 \rightarrow 1$. Its scattering matrix is

$$S = \begin{pmatrix} 0 & 1 & 0 \\ 0 & 0 & 1 \\ 1 & 0 & 0 \end{pmatrix} \tag{1.18}$$

Right-handed and left-handed four port circulators exist as well. Scattering matrices for each are shown in equations 1.19 and 1.20, respectively.

$$S = \begin{pmatrix} 0 & 0 & 0 & 1 \\ 1 & 0 & 0 & 0 \\ 0 & 1 & 0 & 0 \\ 0 & 0 & 1 & 0 \end{pmatrix} \tag{1.19}$$

$$S = \begin{pmatrix} 0 & 1 & 0 & 0 \\ 0 & 0 & 1 & 0 \\ 0 & 0 & 0 & 1 \\ 1 & 0 & 0 & 0 \end{pmatrix} \tag{1.20}$$

Circulators in practice can impart any phase on signals, so the 1s in the scattering matrices could be replaced by complex numbers with unity magnitude. Symbolic representations of each of these circulators are shown in Fig. 1.2. At microwave frequencies, the most common type of circulator is the *ferrite circulator*, which employs the principle of Faraday rotation within a magnetic material to create a nonreciprocal effect. Ferrite devices are bulky and difficult to include in integrated circuits.

1.1.2.2 Isolators

An isolator is a two-port device that only allows transmission of a signal in one direction. An ideal isolator can be described by the scattering matrix

$$S = \begin{pmatrix} 0 & 0 \\ 1 & 0 \end{pmatrix} \tag{1.21}$$

Much like circulators, isolators are most often built with ferrite materials. The functionality of an isolator can be achieved by terminating one of the ports of a three-port circulator with a matched load. A schematic representation of this is shown in Fig. 1.3. Isolators suffer from the same limitations circulators do, since their operation is very similar.

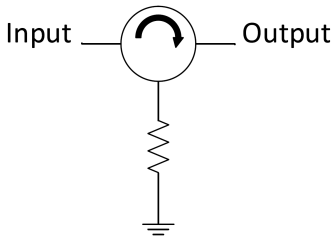

Figure 1.3: An isolator constructed from a circulator. The value of the resistance is the same as the system impedance.

1.1.2.3 Gyrators

First proposed as a new network element by B. D. H. Tellegen in 1948 [11], the gyrator is a nonreciprocal element described by the scattering matrix

$$S = \begin{pmatrix} 0 & 1 \\ -1 & 0 \end{pmatrix} \tag{1.22}$$

A gyrator can essentially be seen as a nonreciprocal phase shifter. In one direction of transmission, the signal emerges in phase. In the opposite direction, the signal emerges with a 180° phase shift. A versatile element, the gyrator is a fundamental nonreciprocal element that can be used to construct other nonreciprocal elements. Shown in Fig. 1.4 is Tellegen's symbol for a gyrator, as well as two circulator configurations that can be realized using a single gyrator.

1.1.3 Noise in Microwave Systems

To appreciate the value of low-noise reciprocal components, it is important to understand the impact of a component on the noise performance of a system. The effect of noise in microwave systems is often characterized by the *noise factor*. Defining $\mathrm{SNR}_{\mathrm{input}}$ as the signal-to-noise ratio at the input and $\mathrm{SNR}_{\mathrm{output}}$ as the signal-to-noise ratio at the output, noise factor can be defined as

$$F = \frac{\mathrm{SNR}_{\mathrm{input}}}{\mathrm{SNR}_{\mathrm{output}}} \tag{1.23}$$

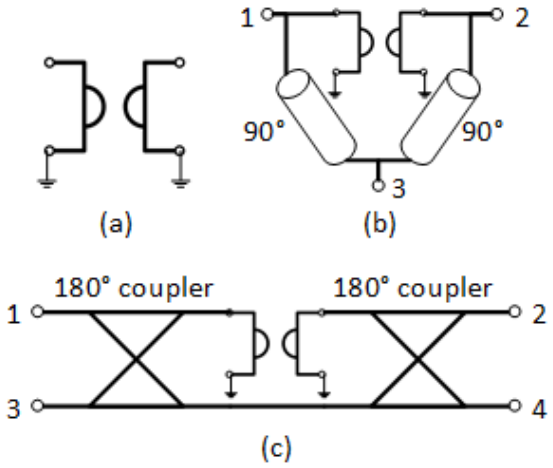

Figure 1.4: (a) Tellegen's symbol for a gyrator. (b) Three-port circulator from gyrator. (c) Four-port circulator from gyrator.

When expressed in a decibel scale, this quantity is referred to as the *noise figure*. Often, a microwave system is modeled as a cascade of individual two-port networks that can represent devices such as amplifiers, mixers, filters and so forth. This model can be used to estimate G_A, the available gain, and F, the noise factor, of the entire network. The definition of available gain is

$$G_A = \frac{P_{avn}}{P_{avs}} \tag{1.24}$$

P_{avs} represents the available source power and P_{avn} represents the available power from the two port network on the output side. With this definition, a load connected to a two-port network sees the network as a source whose available power has been transformed by the gain of the network. Using this property, it is possible to compute the overall available gain of cascade of n two-port networks by taking the product of each network's available gain. In other words, if the overall available gain is $G_{A,\text{total}}$ and the available gain of the ith network is $G_{A,i}$, then

$$G_{A,\text{total}} = \prod_{i=1}^{n} G_{A,i} \tag{1.25}$$

If in this cascade of n two-port netwoks, the ith network has a noise factor

of F_i, then the overall noise factor of the entire system [10] can be expressed as

$$F_{\text{total}} = F_1 + \frac{F_2 - 1}{G_{A,1}} + \frac{F_3 - 1}{G_{A,1}G_{A,2}} + ... + \frac{F_n - 1}{G_{A,1}G_{A,2}G_{A,3}...G_{A,n}} \tag{1.26}$$

The most critical result of this formula is that devices present near the front-end of a microwave system contribute the most to the overall noise factor of the system. It is therefore paramount to minimize the noise figure of the first stage of the system. Perhaps the most well-known example where a nonreciprocal component is placed on the front end of a system is the full-duplex transceiver. A block diagram of this transceiver is shown in Fig. 1.5.

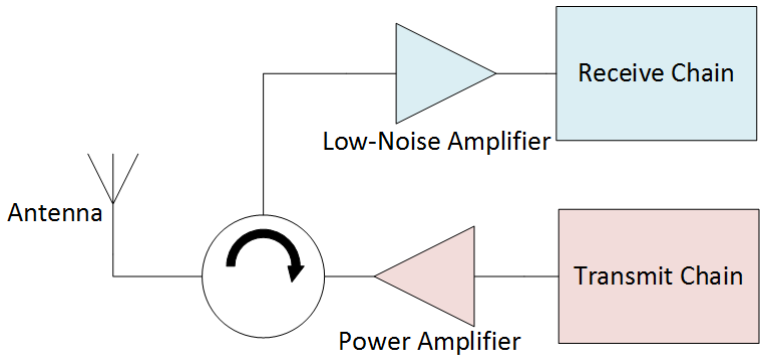

Figure 1.5: A full-duplex transceiver. A circulator separates the transmit and receive chains.

A circulator is placed on the front end of the transceiver to isolate the transmit and receive chains. This allows transmission and reception of signals at the same time and at the same frequency. The noise factors of the antenna, circulator and low-noise amplifier are F_{ANT}, $F_{\text{circulator}}$ and F_{LNA}, respectively. The circulator has unity gain and the low-noise amplifier has a gain of G_{LNA}. The total noise factor F_{RX} of the receiver after the low-noise amplifier is given by

$$F_{\text{RX}} = F_{\text{ANT}} + F_{\text{circulator}} + \frac{F_{\text{LNA}} - 1}{G_{\text{LNA}}} \tag{1.27}$$

This example illustrates the importance of low-noise nonreciprocal compo-

nents.

1.2 Scope of this Research

This thesis concerns the mathematical analysis of a gyrator constructed from parametric devices. This particular gyrator was first explored by A. K. Kamal [12] in 1960 with supporting experimental results, but only a first-order analysis was performed demonstrating the principle of operation. This work seeks to further explore the parametric gyrator by performing an analysis of the effect of nonidealities of nonlinear reactance elements on the insertion loss and noise performance. The results of this analysis are then used to estimate the performance of the parametric gyrator when operating as a circulator. The bandwidth of the circulator is explored, as well as various topologies that can be utilized to physically realize it in both three- and four-port form. Finally, a design example along with simulations is presented to demonstrate the application of the theory presented in the construction of a parametric circulator.

CHAPTER 2

LITERATURE REVIEW

In order to understand the application of parametric circuits to the creation of nonreciprocal elements, an understanding of the operation of parametric circuits is necessary. In this section, the fundamentals of time-varying reactance circuits are explored from the quintessential literature on the subject.

2.1 Analysis of Circuits with Time-Varying Reactance

The seminal two-part paper by J. M. Manley and H. E. Rowe [13, 14] is the fundamental reference in the design of circuits with time-varying reactance, referred to as *parametric* circuits. In the first part, Manley uses a Fourier expansion of the charge on a nonlinear capacitor to derive general energy relations that characterize the power in all frequencies that are generated when the capacitor is driven with two signals of two incommensurate frequencies. In the second paper, Rowe confirms the findings of the first paper by approaching the nonlinear capacitor with small-signal circuit analysis. This part contains information that is paramount in designing physical parametric circuits that are conjugately matched at all ports and provide bilateral frequency conversion.

2.1.1 General Energy Relations

The analysis in both papers assumes the time-varying element is a capacitor with a voltage v that is an arbitrary single-valued function of the charge,

q.

$$v = f(q) \tag{2.1}$$

If two signals of frequencies ω_0 and ω_1 are applied to the capacitor, in general, currents of frequencies $\omega_{mn} = m\omega_0 + n\omega_1$, where m and n take on all integer values, will be generated. In this case, the time-varying charge $q(t)$ flowing through the capacitor can be expressed as a double Fourier series:

$$q(t) = q(\omega_0 t, \omega_1 t) = \sum_{m=-\infty}^{\infty} \sum_{n=-\infty}^{\infty} Q_{mn} e^{j(m\omega_0 t + n\omega_1 t)} \tag{2.2a}$$

$$Q_{mn} = \frac{1}{4\pi^2} \int_0^{2\pi} \int_0^{2\pi} q(\omega_0 t, \omega_1 t) e^{-j(m\omega_0 t + n\omega_1 t)} d(\omega_0 t) d(\omega_1 t) \tag{2.2b}$$

The voltage $v(t)$ across the capacitor is a periodic function, as $f(q(t))$ is a single-valued function. The current $i(t)$ through the capacitor is also periodic, as it is related to the charge as $i(t) = \frac{dq(t)}{dt}$. Thus, both can be expanded using a Fourier series:

$$i(t) = i(\omega_0 t, \omega_1 t) = \frac{dq}{dt} = \sum_{m=-\infty}^{\infty} \sum_{n=-\infty}^{\infty} j(m\omega_0 + n\omega_1) Q_{mn} e^{j(m\omega_0 t + n\omega_1 t)} \tag{2.3}$$

$$v(t) = v(\omega_0 t, \omega_1 t) = \sum_{m=-\infty}^{\infty} \sum_{n=-\infty}^{\infty} V_{mn} e^{j(m\omega_0 t + n\omega_1 t)} \tag{2.4a}$$

$$V_{mn} = \frac{1}{4\pi^2} \int_0^{2\pi} \int_0^{2\pi} f(q(\omega_0 t, \omega_1 t)) e^{-j(m\omega_0 t + n\omega_1 t)} d(\omega_0 t) d(\omega_1 t) \tag{2.4b}$$

By multiplying 2.4b by jmQ^*_{mn}, and defining $I_{mn} = j(m\omega_0 + n\omega_1)Q_{mn}$, then equation 2.5 is obtained after a summation over all m and n is applied.

$$\sum_{m=-\infty}^{\infty}\sum_{n=-\infty}^{\infty} jmQ^*_{mn}V_{mn} = \sum_{m=-\infty}^{\infty}\sum_{n=-\infty}^{\infty}\frac{mV_{mn}I^*_{mn}}{m\omega_0+n\omega_1} = \frac{1}{4\pi^2}\left(\int_0^{2\pi}\int_0^{2\pi} f(q(\omega_0 t,\omega_1 t))e^{-j(m\omega_0 t+n\omega_1 t)}d(\omega_0 t)d(\omega_1 t)\right)\times \left(\sum_{m=-\infty}^{\infty}\sum_{n=-\infty}^{\infty} jmQ^*_{mn}e^{-j(m\omega_0 t+n\omega_1 t)}\right) \quad (2.5)$$

Another similar expression, given in 2.6, can be obtained by multiplying equation 2.4b by jnQ^*_{mn}.

$$\sum_{m=-\infty}^{\infty}\sum_{n=-\infty}^{\infty} jnQ^*_{mn}V_{mn} = \sum_{m=-\infty}^{\infty}\sum_{n=-\infty}^{\infty}\frac{nV_{mn}I^*_{mn}}{m\omega_0+n\omega_1} = \frac{1}{4\pi^2}\left(\int_0^{2\pi}\int_0^{2\pi} f(q(\omega_0 t,\omega_1 t))e^{-j(m\omega_0 t+n\omega_1 t)}d(\omega_0 t)d(\omega_1 t)\right)\times \left(\sum_{m=-\infty}^{\infty}\sum_{n=-\infty}^{\infty} jnQ^*_{mn}e^{-j(m\omega_0 t+n\omega_1 t)}\right) \quad (2.6)$$

These two expressions seem daunting at first glance, but two relations can be found by observing equation 2.2a:

$$\frac{dq}{d(\omega_0 t)} = \sum_{m=-\infty}^{\infty}\sum_{n=-\infty}^{\infty} mQ^*_{mn}e^{-j(m\omega_0 t+n\omega_1 t)} \quad (2.7)$$

$$\frac{dq}{d(\omega_1 t)} = \sum_{m=-\infty}^{\infty}\sum_{n=-\infty}^{\infty} nQ^*_{mn}e^{-j(m\omega_0 t+n\omega_1 t)} \quad (2.8)$$

$\frac{dq}{d(\omega_0 t)}$ is just dq with $\omega_1 t$ held constant, and $\frac{dq}{d(\omega_1 t)}$ is just dq with $\omega_0 t$ held constant. Taking this fact, as well as ignoring the existence of negative frequencies, equations 2.5 and 2.6 can be expressed respectively as

$$\sum_{m=0}^{\infty}\sum_{n=-\infty}^{\infty}\frac{nV_{mn}I^*_{mn}}{m\omega_0+n\omega_1} = \int_0^{2\pi}\int_{q(0,\omega_1 t)}^{q(2\pi,\omega_1 t)} f(q)\,dq\,d(\omega_1 t) \quad (2.9)$$

$$\sum_{m=-\infty}^{\infty}\sum_{n=0}^{\infty}\frac{nV_{mn}I_{mn}^{*}}{m\omega_0+n\omega_1}=\int_0^{2\pi}\int_{q(\omega_0 t,0)}^{q(\omega_0 t,2\pi)}f(q)\,dq\,d(\omega_0 t) \tag{2.10}$$

Since q is periodic both in $\omega_0 t$ and $\omega_1 t$, and $f(q)$ is single-valued, the right hand sides of both of these expressions vanish. Lastly, the power at frequency $m\omega_0+n\omega_1$ is then defined to be $W_{mn}=V_{mn}I_{mn}^{*}$. The final result is the general energy relations for a parametric circuit, given as

$$\sum_{m=0}^{\infty}\sum_{n=-\infty}^{\infty}\frac{mW_{mn}}{m\omega_0+n\omega_1}=0 \tag{2.11a}$$

$$\sum_{m=-\infty}^{\infty}\sum_{n=0}^{\infty}\frac{nW_{mn}}{m\omega_0+n\omega_1}=0 \tag{2.11b}$$

This is, from a physical standpoint, a statement of conservation of energy. Of most interest to this work is the case referred to as the three-frequency parametric converter. This can be thought of as a single sideband mixer. One frequency is a local oscillator, denoted as ω_{LO}. Another is the IF, denoted as ω_{IF}. The RF, ω_{RF}, then has two possibilities, as shown in Fig. 2.1. If $\omega_{\mathrm{RF}}=\omega_{\mathrm{LO}}+\omega_{\mathrm{IF}}$, this is called the *non-inverting converter*, as the shapes of the spectra centered around ω_{IF} and ω_{RF} are the same. If $\omega_{\mathrm{RF}}=\omega_{\mathrm{LO}}-\omega_{\mathrm{IF}}$, this is called the *inverting converter*, as the shapes of the spectra centered around ω_{IF} and ω_{RF} are mirrored with respect to each other. The difference between an upconverter and a downconverter of either of these types is the roles of f_{IF} and ω_{RF}. For an upconverter, the input frequency is ω_{IF} and the output is ω_{RF}. For a downconverter, the input frequency is f_{RF} and the output frequency is ω_{IF}. The energy relations for each case are as follows.

2.1.1.1 Non-inverting Converter

The non-inverting converter has energy relations that are given by

$$\frac{W_{\mathrm{LO}}}{\omega_{\mathrm{LO}}}+\frac{W_{\mathrm{RF}}}{\omega_{\mathrm{RF}}}=0 \tag{2.12}$$

$$\frac{W_{\mathrm{IF}}}{\omega_{\mathrm{IF}}} + \frac{W_{\mathrm{RF}}}{\omega_{\mathrm{RF}}} = 0 \tag{2.13}$$

where W_{IF} is the power consumed at frequency ω_{IF}, W_{RF} is the power consumed at frequency ω_{RF} and W_{LO} is the power consumed at frequency ω_{LO}. When operating the non-inverting converter as an upconverter, $W_{\mathrm{IF}} > 0$ and $W_{\mathrm{RF}} < 0$, and the power gain is given by

$$G_{\mathrm{NI,+}} = \frac{W_{\mathrm{RF}}}{W_{\mathrm{IF}}} = \frac{\omega_{\mathrm{RF}}}{\omega_{\mathrm{IF}}} \tag{2.14}$$

When operating the non-inverting converter as a downconverter, $W_{\mathrm{IF}} < 0$ and $W_{\mathrm{RF}} > 0$, and the power gain is given by 2.15.

$$G_{\mathrm{NI,-}} = \frac{W_{\mathrm{IF}}}{W_{\mathrm{RF}}} = \frac{\omega_{\mathrm{IF}}}{\omega_{\mathrm{RF}}} \tag{2.15}$$

This means that an upconverter will always have a power gain greater than unity and a downconverter will always have a power gain smaller than unity in the non-inverting case.

2.1.1.2 Inverting Converter

The inverting converter has energy relations that are given by

$$\frac{W_{\mathrm{LO}}}{\omega_{\mathrm{LO}}} + \frac{W_{\mathrm{RF}}}{\omega_{\mathrm{RF}}} = 0 \tag{2.16}$$

$$\frac{W_{\mathrm{IF}}}{\omega_{\mathrm{IF}}} - \frac{W_{\mathrm{RF}}}{\omega_{\mathrm{RF}}} = 0 \tag{2.17}$$

When operating the inverting converter as an upconverter, $W_{\mathrm{IF}} < 0$ and $W_{\mathrm{RF}} < 0$, and the power gain is given by

$$G_{\mathrm{I,+}} = \frac{W_{\mathrm{RF}}}{W_{\mathrm{IF}}} = -\frac{\omega_{\mathrm{RF}}}{\omega_{\mathrm{IF}}} \tag{2.18}$$

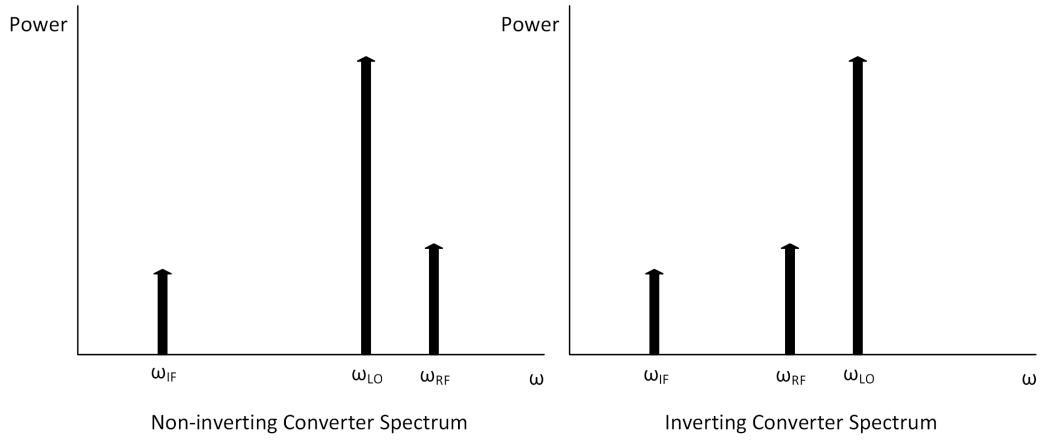

Figure 2.1: Spectra of non-inverting and inverting parametric converter.

When operating the non-inverting converter as a downconverter, $W_{\mathrm{IF}} < 0$ and $W_{\mathrm{RF}} < 0$, and the power gain is given by

$$G_{\mathrm{I,\text{-}}} = \frac{W_{\mathrm{IF}}}{W_{\mathrm{RF}}} = -\frac{\omega_{\mathrm{IF}}}{\omega_{\mathrm{RF}}} \tag{2.19}$$

This represents a potentially unstable system and the transducer gain can take on any value from zero to infinite in both the modulator and demodulator application.

2.1.2 Small-signal Relations for Parametric Circuits

As it was assumed that the voltage v across the nonlinear capacitor is a function of the charge q, it follows that the charge is a function of the voltage. This function is considered the nonlinear capacitance.

$$q = f(v) \tag{2.20}$$

In this analysis, the power of the local oscillator is assumed to be large compared to any other frequency components present in the capacitor. In that case, the operating point is governed solely by the local oscillator, which is to say

$$q_{\mathrm{LO}} = f(v_{\mathrm{LO}}) \tag{2.21}$$

Now the signal component of charge δq and the signal component of voltage δv are much smaller than that of the local oscillator.

$$\delta q = \frac{df(v_{\mathrm{LO}})}{dv}\delta v = \sum_{n=-\infty}^{\infty} C_n e^{jn\omega_{\mathrm{LO}}}\delta v \tag{2.22}$$

Note that $\omega_{\mathrm{LO}} = 2\pi f_{\mathrm{LO}}$. With this assumption, the capacitor can be seen as a linear, time-varying capacitance. Since f is a real-valued function, it follows that $C_n = C_{-n}$ and the time-varying capacitance can be written as

$$C(t) = C_0 + 2C_1\cos(\omega_{\mathrm{LO}}t) + 2C_2\cos(2\omega_{\mathrm{LO}}t) + ... \tag{2.23}$$

Now, if a small signal with angular frequency ω_{IF} is applied and only the fundamental frequency of the local oscillator is considered, δq and δv will contain all frequency components $(n\omega_{\mathrm{LO}} + m\omega_{\mathrm{IF}})$ with m and n taking all integer values including zero. If ideal filters suppress all frequencies but ω_{IF}, $\omega_+ = \omega_{\mathrm{LO}} + \omega_{\mathrm{IF}}$ and $\omega_- = \omega_{\mathrm{LO}} - f_{\mathrm{IF}}$ (assuming, of course, that the local oscillator is still modulating the capacitance), then δq and δv can be expanded using Euler's identity:

$$\delta q = Q_{\mathrm{IF}}e^{j\omega_{\mathrm{IF}}t} + Q^*_{\mathrm{IF}}e^{-j\omega_{\mathrm{IF}}t} + Q_+e^{j\omega_+t} + Q^*_+e^{-j\omega_+t} + Q_-e^{j\omega_-t} + Q^*_-e^{-j\omega_-t} \tag{2.24}$$

$$\delta v = V_{\mathrm{IF}}e^{j\omega_{\mathrm{IF}}t} + V^*_{\mathrm{IF}}e^{-j\omega_{\mathrm{IF}}t} + V_+e^{j\omega_+t} + V^*_+e^{-j\omega_+t} + V_-e^{j\omega_-t} + V^*_-e^{-j\omega_-t} \tag{2.25}$$

The small signal current I through the capacitor can be related to the charge as $I = j\omega Q$ and $I^* = -j\omega Q^*$, and thus an admittance matrix can be ex-

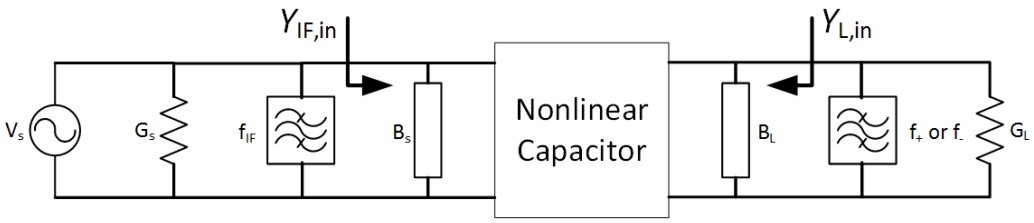

Figure 2.2: Norton equivalent circuit of either non-inverting or inverting parametric converter. The filters are ideally open at the marked frequency and short otherwise. The nonlinear capacitor has an admittance matrix of either equation 2.27 or 2.34.

pressed for this nonlinear capacitor:

$$\begin{bmatrix} I_-^* \\ I_{\mathrm{IF}} \\ I_+ \end{bmatrix} = j \begin{pmatrix} -\omega_- C_0 & -\omega_- C_1 & -\omega_- C_2 \\ \omega_{\mathrm{IF}} C_1 & \omega_{\mathrm{IF}} C_0 & \omega_{\mathrm{IF}} C_1 \\ -\omega_+ C_2 & -\omega_+ C_1 & -\omega_+ C_0 \end{pmatrix} \begin{bmatrix} V_-^* \\ V_{\mathrm{IF}} \\ V_+ \end{bmatrix} \tag{2.26}$$

As stated before, only the fundamental component of the local oscillator modulates the capacitance, so $C_2 = 0$. If the filters are then adjusted to reject either the upper or lower sideband, then the non-inverting and inverting case can be simplified to the Thévenin equivalent circuit of Fig. 2.2.

2.1.2.1 Non-inverting Converter

The admittance matrix of equation 2.26 simplifies to that of equation 2.27 in the non-inverting case, as the signal at ω_- is suppressed.

$$\begin{bmatrix} I_{\mathrm{IF}} \\ I_+ \end{bmatrix} = j \begin{pmatrix} \omega_{\mathrm{IF}} C_0 & \omega_{\mathrm{IF}} C_1 \\ \omega_+ C_1 & \omega_+ C_0 \end{pmatrix} \begin{bmatrix} V_{\mathrm{IF}} \\ V_+ \end{bmatrix} \tag{2.27}$$

With reference to Fig. 2.2, the input admittances at the IF and RF terminals are respectively given by

$$Y_{\mathrm{IF,in}} = j(B_s + \omega_{\mathrm{IF}} C_0) + \frac{\omega_{\mathrm{IF}} \omega_+ C_1^2}{G_L + j(B_L + \omega_+ C_0)} \tag{2.28}$$

$$Y_{\mathrm{L,in}} = j(B_L + \omega_+ C_0) + \frac{\omega_{\mathrm{IF}}\omega_+ C_1^2}{G_L + j(B_L + \omega_{\mathrm{IF}} C_0)} \tag{2.29}$$

The transducer gain of the converter is

$$G_T = \frac{4|\omega_+ C_1|^2 G_S G_L}{|(j(B_S + \omega_{\mathrm{IF}} C_0) + G_S)(j(B_L + \omega_+ C_0) + G_L) + \omega_{\mathrm{IF}}\omega_+ C_1^2|^2} \tag{2.30}$$

This gain is defined as the ratio of the power at the converted frequency to the power available from the source at the input frequency. The reactive components can be removed by choosing the terminal susceptances B_S and B_L to be provided by inductors with values

$$L_S = \frac{1}{\omega_{IF}^2 C_0} \tag{2.31a}$$

$$L_L = \frac{1}{\omega_+^2 C_0} \tag{2.31b}$$

With this selection, the transducer gain reduces to that of equation 2.32.

$$G_T = \frac{4\omega_+^2 C_1^2 G_S G_L}{|G_S + G_L + \omega_{\mathrm{IF}}\omega_+ C_1^2|^2} \tag{2.32}$$

An infinite number of terminal conductances maximize this transducer gain. For instance, if $G_S = G_L = C_1\sqrt{\omega_{\mathrm{IF}}\omega_+}$, then the transducer gain becomes the limit shown in the general energy relations ($G_T = \frac{\omega_+}{\omega_{\mathrm{IF}}}$). In this case, it was implicitly assumed that the converter was an upconverter. If one were to reverse the roles of the terminals, under the same circumstances, the power gain would be $G_T = \frac{\omega_{\mathrm{IF}}}{\omega_+}$. Another consequence of this result is that any system impedance can be matched by either choosing the properties of the nonlinear capacitor or the choice of input and output frequencies. Rowe also estimates the 3 dB fractional bandwidth (FBW) of such a converter as

$$\mathrm{FBW} = \frac{C_1}{C_0}\sqrt{2\frac{\omega_+}{\omega_{\mathrm{IF}}}} \tag{2.33}$$

For a given ω_{IF}, increased bandwidth is obtained with a large modulation depth or a high LO frequency.

2.1.2.2 Inverting Converter

For the inverting converter, the admittance matrix of equation 2.26 simplifies to that of equation 2.34, as the signal at ω_+ is suppressed.

$$\begin{bmatrix} I_{\mathrm{IF}} \\ I_-^* \end{bmatrix} = j \begin{pmatrix} \omega_{\mathrm{IF}} C_0 & \omega_{\mathrm{IF}} C_1 \\ -\omega_- C_1 & -\omega_- C_0 \end{pmatrix} \begin{bmatrix} V_{\mathrm{IF}} \\ V_-^* \end{bmatrix} \tag{2.34}$$

The real part of the input admittance at each port now has the potential to be negative, as shown in equations 2.35 and 2.36. This means the inverting converter is potentially unstable in both the upconverting and downconverting modes of operation.

$$Y_{\mathrm{IF,in}} = j(B_s + \omega_{\mathrm{IF}} C_0) - \frac{\omega_{\mathrm{IF}} \omega_- C_1^2}{G_L + j(B_L + \omega_- C_0)} \tag{2.35}$$

$$Y_{\mathrm{L,in}} = j(B_L + \omega_+ C_0) - \frac{\omega_{\mathrm{IF}} \omega_- C_1^2}{G_L + j(B_L + \omega_{\mathrm{IF}} C_0)} \tag{2.36}$$

If the condition of equation 2.31 is satisfied, then the transducer gain can be expressed as

$$G_T = \frac{4\omega_+^2 C_1^2 G_S G_L}{|G_S + G_L - \omega_{\mathrm{IF}} \omega_+ C_1^2|^2} \tag{2.37}$$

It is noteworthy that $0 < G_T < \infty$. Although this type of frequency converter can yield arbitrary gain in both the upconverter and downconverter modes, these devices often have a negative input resistance, precluding their use as any of the nonreciprocal devices mentioned above. These devices, however, operate well as reflection-type amplifiers.

CHAPTER 3

A PARAMETRIC GYRATOR

Several researchers have found that parametric devices can exhibit nonreciprocal behavior depending on the topology of the device [15, 16, 17]. In this application, it is desired that the device have reciprocal amplitude response, but nonreciprocal phase response. The topology chosen for this gyrator is that explored by A. K. Kamal in 1960 [12], shown in Fig. 3.1. The gyrator is a cascade of two non-inverting parametric converters with the LO inputs of the converters out of phase by 90°. A signal at frequency ω_{IF} entering the gyrator at port 1 is upconverted to a higher frequency (called the *idler frequency*) $\omega_+ = \omega_{\mathrm{IF}} + \omega_{\mathrm{LO}}$ at converter 1. It is then downconverted at converter 2 and emerges from port 2 at ω_{IF} and at some phase θ_{21}. A signal entering the gyrator at port 2 is upconverted to $\omega_+ = \omega_{\mathrm{IF}} + \omega_{\mathrm{LO}}$ at converter 2 and then downconverted at converter 1. The signal emerges from port 1 at ω_{IF} and at some phase θ_{12}. The 90° phase difference between the two LO signals causes $|\theta_{21} - \theta_{12}| = 180°$. Although the transmission phase between ports is frequency dependent, the differential phase shift can be maintained over the entire bandwidth of the device, as the difference in forward and reverse phase shifts is controlled solely by the phase difference between the two LO signals. An ideal model of this gyrator can have a maximum gain of unity. Intuitively, this can be predicted with Manley's general energy relations, as the gain of an upconverter is exactly the reciprocal of that of a downconverter. This can be shown more explicitly using the small-signal analysis of Rowe.

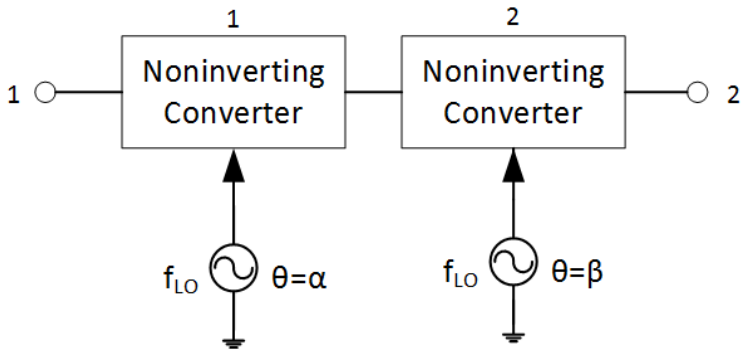

Figure 3.1: Component-level diagram of parametric gyrator.

3.1 Theory of Operation

If the LO in a non-inverting converter is now allowed to have a phase angle θ, then the time-varying capacitance in equation 2.23 can be expressed as in equation 3.1, assuming the fundamental tone of the LO is the only signal modulating the capacitor.

$$C(t) = C_0 + 2C_1 \cos(2\pi f_{\mathrm{LO}} + \theta) \tag{3.1}$$

Considering equation 2.22, it is clear that θ can be considered the phase angle of C_1. Thus, the admittance matrix of equation 2.27 can be rewritten as

$$\begin{bmatrix} I_{\mathrm{IF}} \\ I_+ \end{bmatrix} = j2\pi \begin{pmatrix} f_{\mathrm{IF}} C_0 & f_{\mathrm{IF}} |C_1| e^{j\theta} \\ f_+ |C_1| e^{-j\theta} & f_+ C_0 \end{pmatrix} \begin{bmatrix} V_{\mathrm{IF}} \\ V_+ \end{bmatrix} \tag{3.2}$$

The ABCD matrix formalism is more amenable to analysis of a cascade of two-port networks, and so the matrix of equation 3.2 is expressed in ABCD form as

$$\begin{bmatrix} V_{\mathrm{IF}} \\ I_{\mathrm{IF}} \end{bmatrix} = \begin{pmatrix} e^{-j\theta} & 0 \\ 0 & e^{-j\theta} \end{pmatrix} \begin{pmatrix} -\frac{C_0}{|C_1|} & \frac{j}{\omega_{\mathrm{IF}} |C_1|} \\ j\omega_{\mathrm{IF}} (|C_1| - \frac{C_0^2}{|C_1|}) & -\frac{\omega_{\mathrm{IF}}}{\omega_+} \frac{C_0}{|C_1|} \end{pmatrix} \begin{bmatrix} V_+ \\ I_+ \end{bmatrix} \tag{3.3}$$

In equation 3.3, this represents an upconverter. A downconverter would have

a matrix equal to the inverse of this matrix, or:

$$\begin{bmatrix} V_+ \\ I_+ \end{bmatrix} = \begin{pmatrix} e^{j\theta} & 0 \\ 0 & e^{j\theta} \end{pmatrix} \begin{pmatrix} -\frac{C_0}{|C_1|} & \frac{j}{\omega_{\rm IF}|C_1|} \\ j\omega_{\rm IF}(|C_1| - \frac{C_0^2}{|C_1|}) & -\frac{\omega_{\rm IF}}{\omega_+}\frac{C_0}{|C_1|} \end{pmatrix}^{-1} \begin{bmatrix} V_{\rm IF} \\ I_{\rm IF} \end{bmatrix} \tag{3.4}$$

Now, the overall ABCD matrix of the gyrator can be found by taking the product of each of the ABCD matrices of each converter in Fig. 3.1:

$$\begin{aligned} \begin{bmatrix} V_1 \\ I_1 \end{bmatrix} = &\begin{pmatrix} e^{-j\alpha} & 0 \\ 0 & e^{-j\alpha} \end{pmatrix} \begin{pmatrix} -\frac{C_0}{|C_1|} & \frac{j}{\omega_{\rm IF}|C_1|} \\ j\omega_{\rm IF}(|C_1| - \frac{C_0^2}{|C_1|}) & -\frac{\omega_{\rm IF}}{\omega_+}\frac{C_0}{|C_1|} \end{pmatrix} \times \\ &\begin{pmatrix} e^{j\beta} & 0 \\ 0 & e^{j\beta} \end{pmatrix} \begin{pmatrix} -\frac{C_0}{|C_1|} & \frac{j}{\omega_{\rm IF}|C_1|} \\ j\omega_{\rm IF}(|C_1| - \frac{C_0^2}{|C_1|}) & -\frac{\omega_{\rm IF}}{\omega_+}\frac{C_0}{|C_1|} \end{pmatrix}^{-1} \begin{bmatrix} V_2 \\ I_2 \end{bmatrix} \\ = &\begin{pmatrix} e^{j(\beta-\alpha)} & 0 \\ 0 & e^{j(\beta-\alpha)} \end{pmatrix} \begin{bmatrix} V_2 \\ I_2 \end{bmatrix} \end{aligned} \tag{3.5}$$

The nonreciprocity of the device can be seen more clearly by converting the ABCD matrix to a scattering matrix:

$$[S] = \begin{pmatrix} 0 & e^{j(\beta-\alpha)} \\ e^{j(\alpha-\beta)} & 0 \end{pmatrix} \tag{3.6}$$

If $\alpha = 0$ and $\beta = \frac{\pi}{2}$, then the scattering matrix becomes

$$[S] = j\begin{pmatrix} 0 & 1 \\ -1 & 0 \end{pmatrix} \tag{3.7}$$

This is the function of a gyrator, except there is an additional $\frac{\pi}{2}$ phase delay in each direction, but the differential phase shift is π. In practice, there will be additional phase delay in each direction because of filter networks, tuning elements, etc. but the differential phase is controlled solely by the phase difference of the two LO signals.

3.2 Amplitude Response

When constructing parametric devices, the nonlinear reactance utilized will have some appreciable loss. Assuming the device is constructed using lossless filters, the effect of nonideal reactance on various performance parameters can be estimated. Including the losses in filters and matching elements can be used to model the loss even more accurately if those losses are non-negligible.

3.2.1 Insertion Loss

Insertion loss (IL) of a two-port device is defined as the ratio of output power observed at a port to the input power supplied to the other port, and is expressed in decibel scale. If a two-port network has some transducer gain function G_T, under the condition of conjugate matching at both ports, the transducer gain becomes equal to the available gain, G_A. For a cascade of two-ports each conjugately matched at each port, the total gain of the system is the product of each two-port's available gain. In other words, if there are n two-ports, each with available gain $G_{A,n}$, then the overall available gain $G_{A,\text{network}}$ of the network is

$$G_{A,\text{network}} = \prod_{i=1}^{n} G_{A,n} \tag{3.8}$$

This fact is useful, as the insertion loss of the gyrator can be estimated by deriving the transducer gain of an individual conjugately matched converter, and then taking the product of the transducer gains of two converters. Whether a signal propagates from port 1 to port 2 or vice versa, it will encounter an upconversion stage and then a downconversion stage (although it is possible to design the converter to begin with a downconversion stage and end with an upconversion stage). Therefore, the transducer gains of an upconverter and a downconverter should be explored. Varactors are frequently used in parametric converters, and the loss in a varactor is characterized using a series resistance. It is more convenient, then, to work in terms of the impedance matrix of a non-inverting parametric converter. First, the

time-varying capacitance is re-expressed as

$$C(t) = C_0(1 + 2\psi\cos(\omega_{\mathrm{LO}}t + \theta)) \tag{3.9}$$

where ψ is the modulation parameter, and is restricted to be $0 < \psi < \frac{1}{2}$ so $C(t)$ is positive. The impedance matrix can then be found by inverting the admittance matrix of equation 2.27 after replacing C_1 with $\psi C_0 e^{j\theta}$:

$$\begin{bmatrix} V_{\mathrm{IF}} \\ V_+ \end{bmatrix} = \begin{pmatrix} \frac{1}{j\omega_{\mathrm{IF}}C_0(1-\psi^2)} & \frac{\psi}{j\omega_+C_0(1-\psi^2)}e^{j\theta} \\ \frac{\psi}{j\omega_{\mathrm{IF}}C_0(1-\psi^2)}e^{-j\theta} & \frac{1}{j\omega_+C_0(1-\psi^2)} \end{pmatrix} \begin{bmatrix} I_{\mathrm{IF}} \\ I_+ \end{bmatrix} \tag{3.10}$$

This impedance matrix can be used in the Thévenin equivalent circuit of the parametric converter, shown in Fig. 3.2. The impedance matrix of equation 3.10 represents the two-port network labeled "Nonlinear Capacitor".

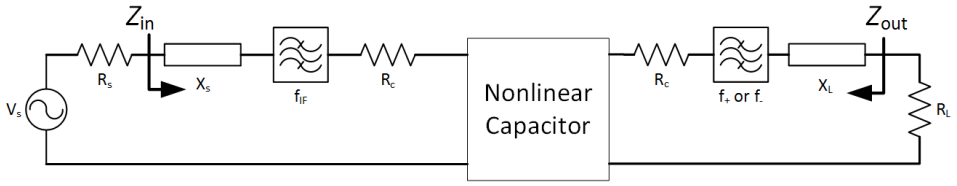

Figure 3.2: Thévenin equivalent circuit of non-inverting parametric converter. The nonlinear capacitor can be represented by the impedance matrix of equation 3.10.

R_S and R_L represent the source and load impedances, respectively. X_S and X_L are the tuning reactances at the source and load, respectively. Filters at the input and output ensure the assumption that only f_{IF} is present at the input and f_+ is present at the output. The loss of the nonlinear capacitor is modeled as a series resistance R_c. To simplify the derivation, it is assumed that the source and load impedances are equal ($R_S = R_L = R$) and purely resistive. The input impedance presented to the source, Z_{in}, can be expressed as

$$Z_{\text{in}} = R_c + j\left(X_S - \frac{1}{\omega_{\text{IF}} C_0(1-\psi^2)}\right) + \frac{1}{\omega_{\text{IF}}\omega_+}\left(\frac{\psi}{C_0(1-\psi^2)}\right)^2 \times \frac{1}{j\left(X_S - \frac{1}{\omega_+ C_0(1-\psi^2)}\right) + R} \tag{3.11}$$

To match the converter at both ports, X_S and X_L should be positive reactances, and so inductors are selected. The reactances can then be written as $X_S = \omega_{\text{IF}} L_S$ and $X_L = \omega_+ L_L$, where L_S and L_L are the source and load tuning inductances, respectively. These inductances are chosen to tune out the static portion of the capacitance, which allows a resistive input impedance and output impedance to be presented to the source and load terminations, respectively.

$$L_S = \frac{1}{\omega_{\text{IF}}^2 C_0(1-\gamma^2)} \tag{3.12}$$

$$L_L = \frac{1}{\omega_+^2 C_0(1-\gamma^2)} \tag{3.13}$$

Under this matching condition, the input impedance reduces to

$$Z_{\text{in}} = R_c + \frac{1}{\omega_{\text{IF}}\omega_+}\left(\frac{\psi}{C_0(1-\psi^2)}\right)^2\left(\frac{1}{R+R_c}\right) \tag{3.14}$$

The transducer gain under the matching condition can be expressed as

$$G_T = \frac{4|Z_{21}|^2 R^2}{|Z_{\text{in}} Z_{\text{out}} - Z_{12} Z_{21}|^2} = \frac{4R^2 \frac{\psi^2}{\omega_{\text{IF}}^2 C_0^2 (1-\psi^2)^2}}{(R^2 + R_c^2 + 2RR_c + \frac{\psi^2}{\omega_{\text{IF}}\omega_+ C_0^2(1-\psi^2)^2})^2} \tag{3.15}$$

with Z_{out} defined as

$$Z_{\text{out}} = R_c + \frac{1}{\omega_{\text{IF}}\omega_+}\left(\frac{\psi}{(C_0(1-\psi^2))}\right)^2\left(\frac{1}{R+R_c}\right) \tag{3.16}$$

The symmetry of the equivalent circuit causes $Z_{\text{in}} = Z_{\text{out}}$, meaning both ports can be conjugately matched. To find the optimum source and load terminations, the derivative of the transducer gain is taken with respect to R and then set to zero.

$$\frac{dG_T}{dR} = \frac{8\frac{\psi^2}{\omega_{\text{IF}}^2 C_0^2(1-\psi^2)^2}R(\frac{\psi^2}{\omega_{\text{IF}}\omega_+ C_0^2(1-\psi^2)^2} + R_c^2 - R^2)}{(\frac{\psi^2}{\omega_{\text{IF}}\omega_+ C_0^2(1-\psi^2)^2} + (R_c+R)^2)^3} = 0 \tag{3.17}$$

The value of R that satisfies this condition is given by

$$R_S = R_L = R_c\sqrt{1 + \frac{\psi^2}{\omega_{\text{IF}}\omega_+ R_c^2 C_0^2(1-\psi^2)^2}} \tag{3.18}$$

With this selection of R, at the center frequency of operation, $Z_{\text{in}} = Z_{\text{out}} = R$. This is exactly the condition for conjugate matching at both ports. In order to characterize the lossy behavior of a varactor, the *dynamic quality factor*, Q_{d}, is introduced:

$$Q_{\text{d}} = \frac{1}{\omega_{\text{IF}} R_c C_0(1-\psi^2)} \tag{3.19}$$

Much like the ubiquitous figure of merit Q of an ordinary resonator, a large value of Q_{d} indicates a low-loss device. A device with $Q_{\text{d}} = \infty$ is lossless, and one would expect the transducer gain of such a device to be $\frac{f_+}{f_{\text{IF}}}$. Using this new definition, G_T as defined in equation 3.15 can be rewritten.

$$G_T = \frac{(1+\frac{\omega_{\text{IF}}}{\omega_+}\psi^2 Q_{\text{d}}^2)Q_{\text{d}}^2\psi^2}{((1+\frac{\omega_{\text{IF}}}{\omega_+}\psi^2 Q_{\text{d}}^2) + \sqrt{1+\frac{\omega_{\text{IF}}}{\omega_+}\psi^2 Q_{\text{d}}^2})^2} \tag{3.20}$$

Now, a new parameter, ξ, called the *dynamic loss factor* is defined:

$$\xi^2 = \frac{f_+}{f_{\text{IF}}}\frac{1}{(\psi Q_{\text{d}})^2} \tag{3.21}$$

The transducer gain can then be rearranged to be in terms of this new parameter.

$$G_T = \frac{\omega_+}{\omega_{\mathrm{IF}}} \frac{1}{(\xi + \sqrt{1+\xi^2})^2} \tag{3.22}$$

When $\xi = 0$, the transducer gain is $\frac{f_+}{f_{\mathrm{IF}}}$ for an upconverter and $\frac{f_{\mathrm{IF}}}{f_+}$ for a downconverter, the result for a lossless parametric converter following the formalism of Manley and Rowe (recall that an upconverter has an input frequency f_{IF} and an output frequency of f_+, but a downconverter has the opposite). This is also apparent because $\xi = 0$ when $Q_{\mathrm{d}} = \infty$. Returning to the discussion of the gyrator of Fig. 3.1, when both converters are conjugately matched at both ports, each converter's transducer gain G_T becomes equal to its available gain G_A, and thus the insertion loss of the gyrator is the product of the transducer gain of an upconversion stage, $G_\uparrow$, and the transducer gain of a downconversion stage, $G_\downarrow$.

$$G_\uparrow = \frac{\omega_+}{\omega_{\mathrm{IF}}} \frac{1}{(\xi + \sqrt{1+\xi^2})^2} \tag{3.23}$$

$$G_\downarrow = \frac{\omega_{\mathrm{IF}}}{\omega_+} \frac{1}{(\xi + \sqrt{1+\xi^2})^2} \tag{3.24}$$

The insertion loss is then expressed as

$$\mathrm{IL} = G_\uparrow G_\downarrow = \frac{1}{(\xi + \sqrt{1+\xi^2})^4} \tag{3.25}$$

Although this analysis was performed assuming the initial stage of the gyrator is an upconverter and the final stage is a downconverter, the results are identical in the case that the first stage is an upconverter and the last stage is a downconverter. This is because the product of transducer gains is commutative, meaning $G_\uparrow G_\downarrow = G_\downarrow G_\uparrow$. In Fig. 3.3, the insertion loss of the gyrator is plotted over dynamic quality factor for various conversion ratios ($\frac{\omega_+}{\omega_{\mathrm{IF}}}$).

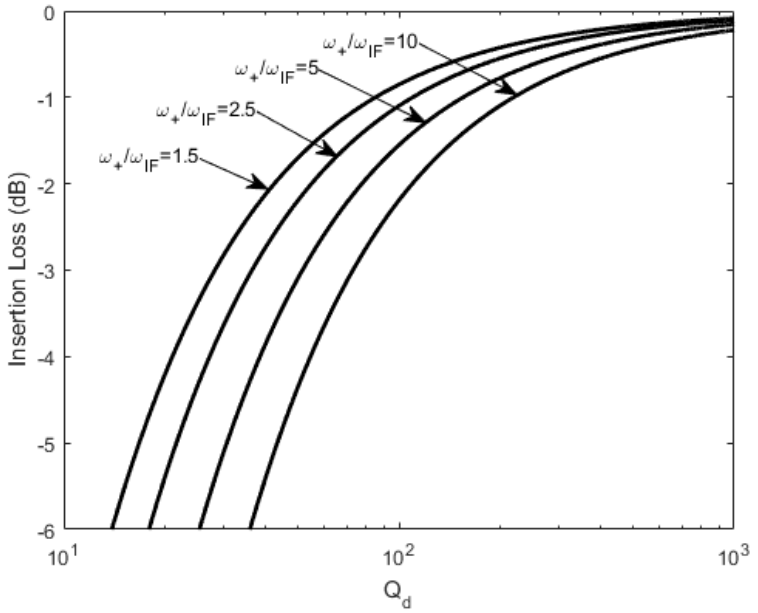

Figure 3.3: Insertion loss of gyrator for various conversion ratios with ψ fixed at 0.25.

3.3 Noise Performance

The noise performance of variable capacitance devices was investigated by many researchers, including Kurokawa and Uenohara [18]. Although the analysis was performed for parametric amplifiers, the discussion is still relevant here. Since it is required that a gyrator is matched at both ports, the noise figure under matched conditions is considered. Since the only dissipative element in the nonlinear capacitor is the series resistance R_c, it is the only element that contributes noise aside from the terminations. Considering just a signal converter stage under matched conditions, the circuit model of Fig. 3.2 can be reformulated as that of Fig. 3.4. The values of R_{CAP}, $A_{\uparrow}$ and $A_{\downarrow}$ are

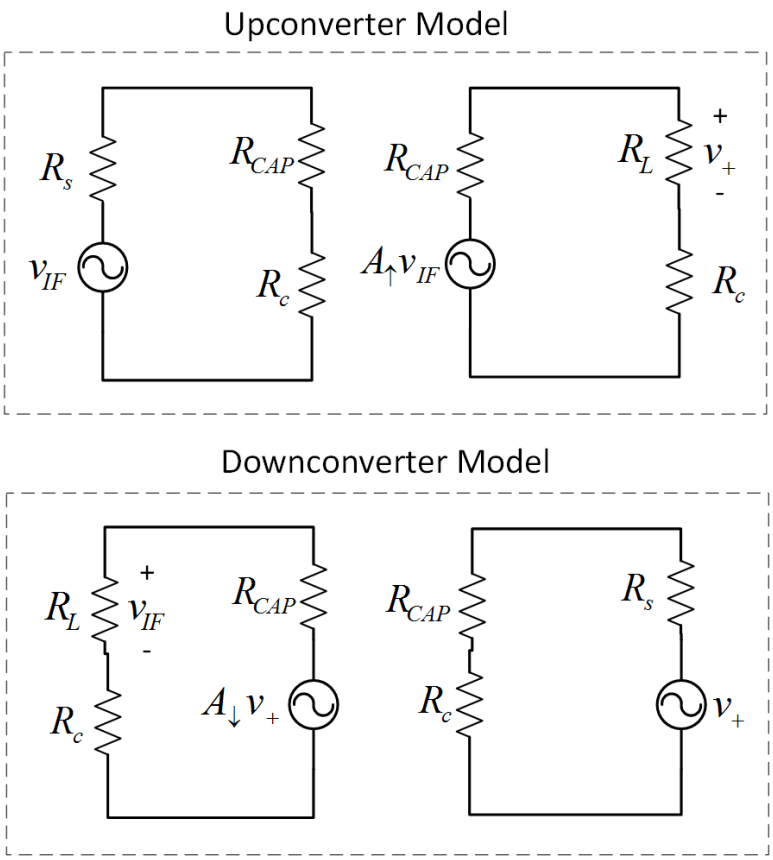

Figure 3.4: Equivalent noise model of both upconverter and downconverter.

$$R_{\mathrm{CAP}} = \frac{\psi^2}{(R+R_c)\omega_{\mathrm{IF}}\omega_+ C_0^2(1-\psi^2)^2} \tag{3.26a}$$

$$|A_\uparrow|^2 = \frac{\omega_+}{\omega_{\mathrm{IF}}} \frac{1}{(\xi+\sqrt{1+\xi^2})^2} \tag{3.26b}$$

$$|A_\downarrow|^2 = \frac{\omega_{\mathrm{IF}}}{\omega_+} \frac{1}{(\xi+\sqrt{1+\xi^2})^2} \tag{3.26c}$$

The noise factor (F) is then defined as the ratio of the SNR across the input resistance to the SNR across the output resistance. As in Fig. 3.4, the upconverter and downconverter are considered as separate cases, as the roles of the terminations as input and output are different in these cases. In general, the noise factor can be expressed as in equation 3.27 where $P_{s,\mathrm{IN}}$ is the input signal power, $P_{s,\mathrm{OUT}}$ is the output signal power, $P_{N,\mathrm{OUT}}$ is the noise output power and $P_{N,\mathrm{IN}}$ is the noise input power.

$$F = \frac{\mathrm{SNR_{IN}}}{\mathrm{SNR_{OUT}}} = \frac{P_{s,\mathrm{IN}}}{P_{s,\mathrm{OUT}}} \times \frac{P_{N,\mathrm{OUT}}}{P_{N,\mathrm{IN}}} \tag{3.27}$$

3.3.1 Parametric Modulator Noise Factor

In reference to Fig. 3.4, the noise factor can be found for an upconverter by taking 3.27 and rewriting it as

$$F_{\uparrow} = \frac{1}{|A_{\uparrow}|^2} \times \frac{P_{N,\mathrm{OUT}}}{P_{N,\mathrm{IN}}} \tag{3.28}$$

Since the ratio of the output to input noise power is needed, finding the square RMS noise voltage at both the input and output is sufficient to compute this ratio. The square RMS noise voltage at the input, $v^2_{\mathrm{N,in,RMS}}$, is the familiar quantity $4kTBR_s$, where k is Boltzmann's constant, T is the physical temperature and B is the measurement bandwidth. The square RMS output noise voltage, $v^2_{\mathrm{N,out,RMS}}$, at the output can then be found from the upconverter model.

$$v^2_{\mathrm{N,out,RMS}} = 4kTB\bigg(R_c + R_L + |A_{\uparrow}|^2(R_s + R_c)\bigg) \tag{3.29}$$

Applying the matching condition of 3.18, this can be further simplified:

$$v^2_{\mathrm{N,out,RMS}} = 4kTBR_c\bigg(1 + \sqrt{1 + \frac{1}{\xi^2}}\bigg)\bigg(1 + |A_{\uparrow}|^2\bigg) \tag{3.30}$$

Now, the noise factor, $F_{\uparrow}$, can be found from these quantities:

$$\begin{aligned} F_{\uparrow} &= \frac{1}{|A_{\uparrow}|^2} \times \frac{v^2_{\mathrm{N,out,RMS}}}{v^2_{\mathrm{N,in,RMS}}} \\ &= 1 + \frac{\xi}{\sqrt{1+\xi^2}} + \frac{\omega_{\mathrm{IF}}}{\omega_+}\bigg(1 + \frac{\xi}{\sqrt{1+\xi^2}}\bigg)\bigg(\xi + \sqrt{1+\xi^2}\bigg)^2 \end{aligned} \tag{3.31}$$

For a downconverter, the same procedure can be utilized to find the noise

factor, $F_{\downarrow}$:

$$F_{\downarrow} = 1 + \frac{\xi}{\sqrt{1+\xi^2}} + \frac{\omega_+}{\omega_{\mathrm{IF}}}\left(1 + \frac{\xi}{\sqrt{1+\xi^2}}\right)\left(\xi + \sqrt{1+\xi^2}\right)^2 \tag{3.32}$$

If the modulation parameter ψ is held fixed, a lower noise factor is achieved using a higher LO frequency (as $\omega_+ = \omega_{\mathrm{IF}} + \omega_{\mathrm{LO}}$) for an upconverter, but this is the opposite for a downconverter. This is evident in Fig. 3.5. If the LO frequency is fixed, then a deeper modulation depth (larger value of ψ) can achieve a somewhat lower noise factor. This is demonstrated in Fig. 3.6 for both an upconverter and downconverter.

3.3.2 Gyrator Noise Factor

Since the upconverter has a lower noise factor and provides gain, it is fairly obvious that a gyrator whose first stage is an upconverter and second stage is a downconverter yields the lowest noise factor. For that reason, only this case is investigated. It is trivial to find this noise factor, F_{gyrator}, using the Friis formula of equation 1.25. The expression is more convenient when written in terms of the insertion loss (IL) defined in equation 3.25:

$$\begin{aligned} F_{\mathrm{gyrator}} &= F_{\uparrow} + \frac{F_{\downarrow} - 1}{|A_{\uparrow}|^2} \\ &= \frac{\omega_{\mathrm{IF}}}{\omega_+}\frac{1}{\sqrt{\mathrm{IL}}} + 2\left[1 + \frac{\xi}{\sqrt{1+\xi^2}}\left(1 + \frac{\omega_{\mathrm{IF}}}{\omega_+}\frac{1}{\sqrt{\mathrm{IL}}}\right)\right] \end{aligned} \tag{3.33}$$

In the losssless case, $\xi = 0$ and IL $= 1$, which reduces the gyrator noise factor to $2 + \frac{\omega_{\mathrm{IF}}}{\omega_+}$. As a brief example, for conversion ratios ($\frac{\omega_+}{\omega_{\mathrm{IF}}}$) of 1.5, 3 and 5, the noise figures would be 4.26 dB, 3.68 dB and 3.42 dB, respectively. Of course, this derivation assumes the only contributor to noise by the nonlinear capacitor itself is the series loss resistance R_c, but nonlinear capacitors are often implemented using varactor diodes. In this case, other factors such as shot noise would need to be considered. In a design situation, typically the

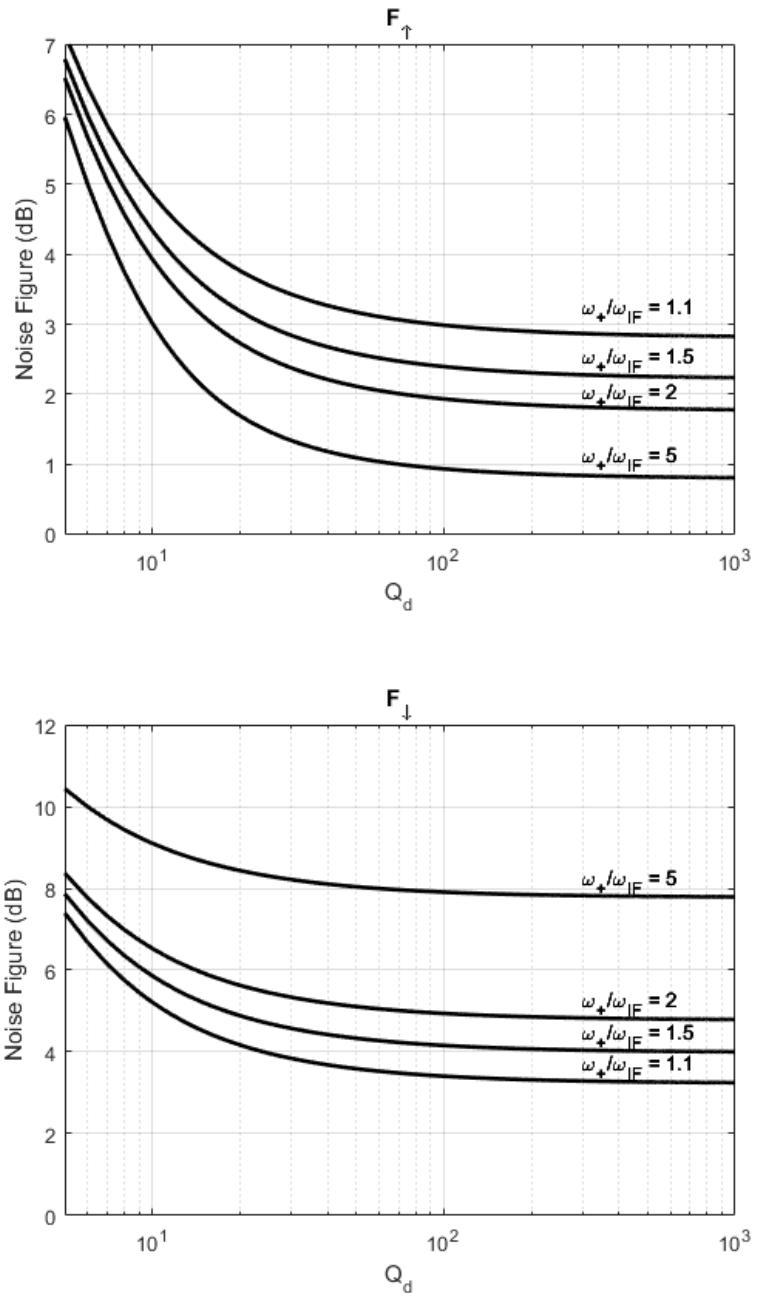

Figure 3.5: Noise figure for a fixed modulation parameter ($\psi = 0.25$) for an upconverter ($F_{\uparrow}$) and a downconverter ($F_{\downarrow}$).

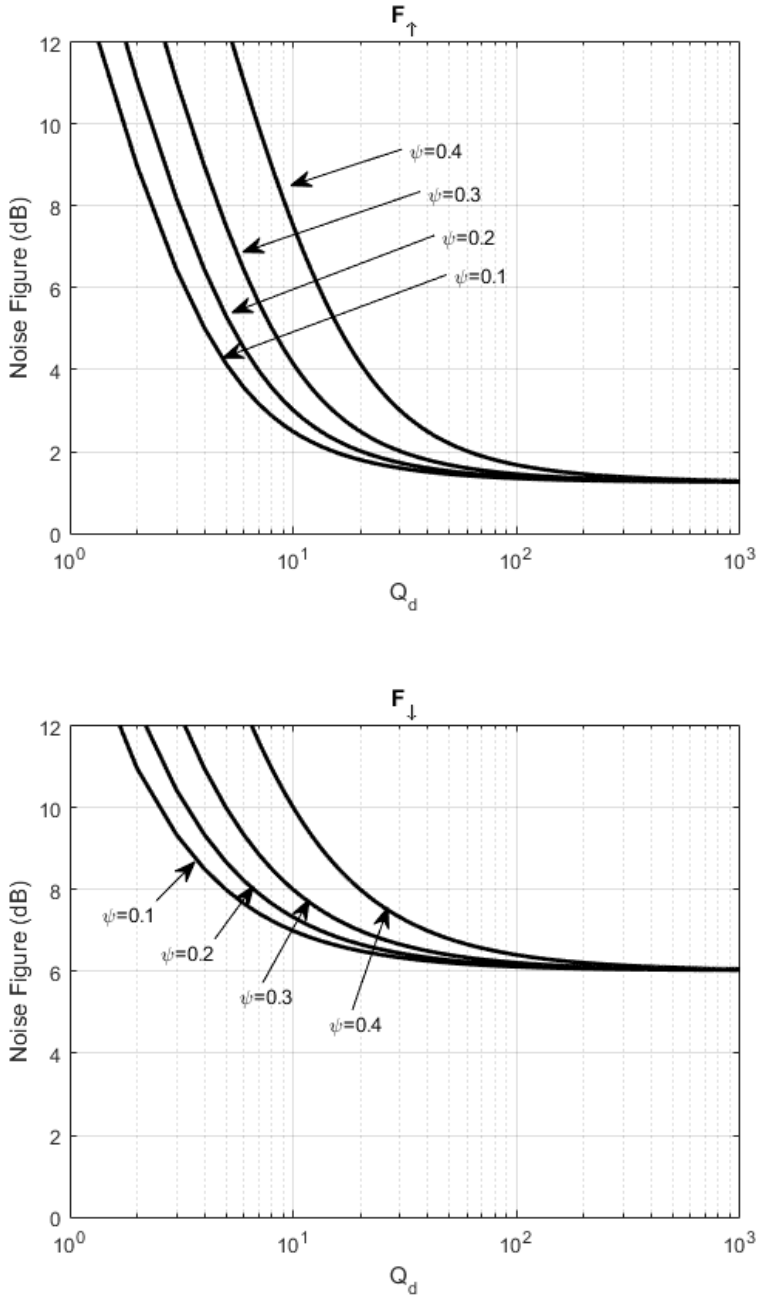

Figure 3.6: Noise figure for a fixed frequency ratio ($\frac{\omega_+}{\omega_{IF}} = 3$) for an upconverter ($F_\uparrow$) and a downconverter ($F_\downarrow$).

value of ψ is fixed at some maximum value supported by a variable capacitor, and so it is most useful to analyze a gyrator with a fixed value of ψ. Shown in Fig. 3.7 is the gyrator noise figure over the frequency conversion ratio $\frac{\omega_+}{\omega_{\mathrm{IF}}}$ for various values of Q_{d}. The modulation parameter ψ is held fixed at 0.25. It is noteworthy that when the dynamic quality factor is fixed (which is a typical situation where the design frequency and nonlinear capacitor properties cannot be changed), there is a conversion ratio that minimizes the noise figure. This implies that the LO frequency should be carefully chosen if minimum noise figure is imperative in a design.

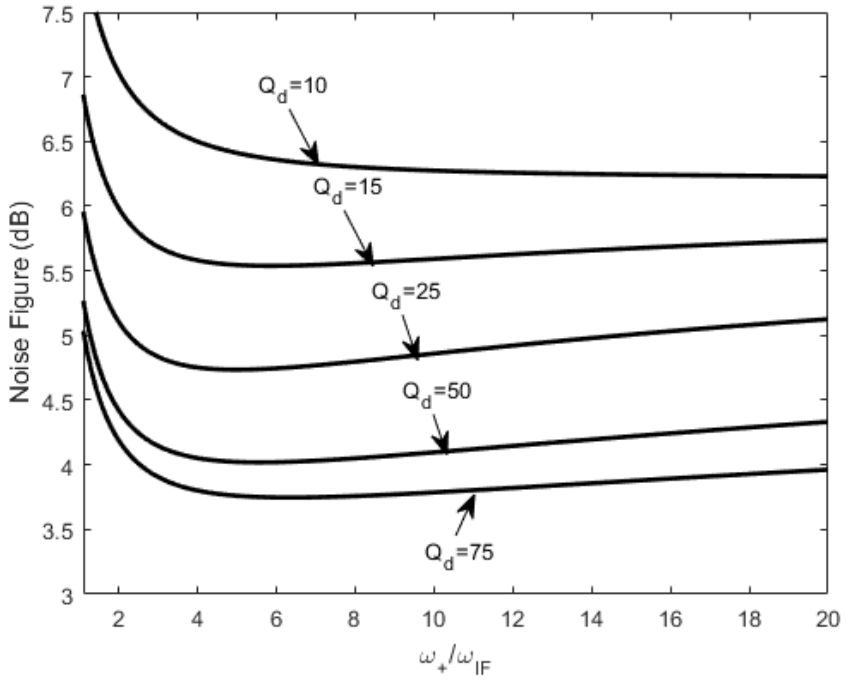

Figure 3.7: Noise figure of gyrator with various Q_{d} with ψ fixed at 0.25.

CHAPTER 4

ANALYSIS OF A FOUR-PORT PARAMETRIC GYRATOR-CIRCULATOR

As was discussed and shown in Fig. 1.4, circulators can be constructed from gyrators, but the topologies shown only function properly for the ideal circulator. When physically realized, the topologies must be adjusted to be compatible with the nonidealities of the device. In both of the topologies, circulation is achieved between port pairs by evenly dividing a signal incident upon some port into two paths with one path having reciprocal phase and another path having nonreciprocal phase. When the signal recombines at the other port, it is combined either in phase or out of phase depending on the direction of transmission. This mechanism requires that both paths have the same time delay in order for the split signal to combine properly. This is easily achieved in the topology of Fig. 1.4 (c) due to the symmetry of the topology, but it is not so readily achieved in Fig. 1.4 (b). For this reason, this section focuses primarily on the topology of Fig. 1.4 (c). It is of interest to develop a method to estimate the time delay of the gyrator in order to compensate for the effect. In addition, this circulator is bandwidth limited, as the 180° phase balance between coupled ports in the hybrid coupler is only maintained at the center frequency. The hybrid couplers only maintain equal power division between coupled ports over a limited range as well. The gyrator itself may limit the useful isolation bandwidth of the circulator if its own amplitude bandwidth is limited. In the work of Manley and Rowe, it was found that having a high conversion ratio $\frac{\omega_+}{\omega_{\mathrm{IF}}}$ can yield a higher amplitude bandwidth, and the noise analysis of the previous chapter found that in general, up to a certain point, higher conversion ratios yield a lower noise figure.

4.1 Theory of Operation

As stated before, the parametric gyrator relies on cancellation of signals to achieve isolation at various ports. There are essentially two elements that comprise the four-port circulator. The first element is a passive, recriprocal power divider/combiner known as a 180° hybrid coupler. The other is the nonreciprocal component, which is the parametric gyrator.

4.1.1 The 180° Hybrid Coupler

The 180° hybrid coupler, henceforth referred to as a *hybrid* for brevity, is a common component in microwave engineering. It is a four-port passive device that can be realized in many forms, such as a waveguide magic tee or a microstrip ratrace coupler. Although various properties of the hybrid (such as bandwidth) are dependent its realization, the function is the same irrespective of implementation. The ideal scattering matrix of the hybrid at its center frequency is

$$S = \frac{-j}{\sqrt{2}} \begin{pmatrix} 0 & 1 & 1 & 0 \\ 1 & 0 & 0 & -1 \\ 1 & 0 & 0 & 1 \\ 0 & -1 & 1 & 0 \end{pmatrix} \tag{4.1}$$

For any given port, the remaining three ports are termed the *sum* port (represented with the symbol Σ), the *difference* port (represented with the symbol Δ) and the *isolated* port. When a signal is sent through a port, the hybrid divides it equally between the sum and difference ports. The divided signals are in phase with each other. The isolated port ideally has no signal exit. For example, if a signal is sent into port 1 of the hybrid, port 2 is the sum port, port 3 is the difference port and port 4 is the isolated port. Alternatively, the hybrid can operate as a combiner. Now, if a signal is applied to both the input port and isolated port, the sum port outputs the sum of the two signals and the difference port outputs the difference of the two signals. Using the same example as before, if two equal power, in-phase signals are applied to ports 1 and 4 each, then port 2 outputs the sum of the

two signals and port 3 should output no signal, since the difference between the two signals is zero. Figure 4.1 shows the system-level symbol commonly used for a hybrid, as well as a pictorial representation of the magic tee and the microstrip ratrace hybrid. In Kamal's work, the hybrid of choice was the magic tee, as parametric modulators were often constructed in waveguide form at the time.

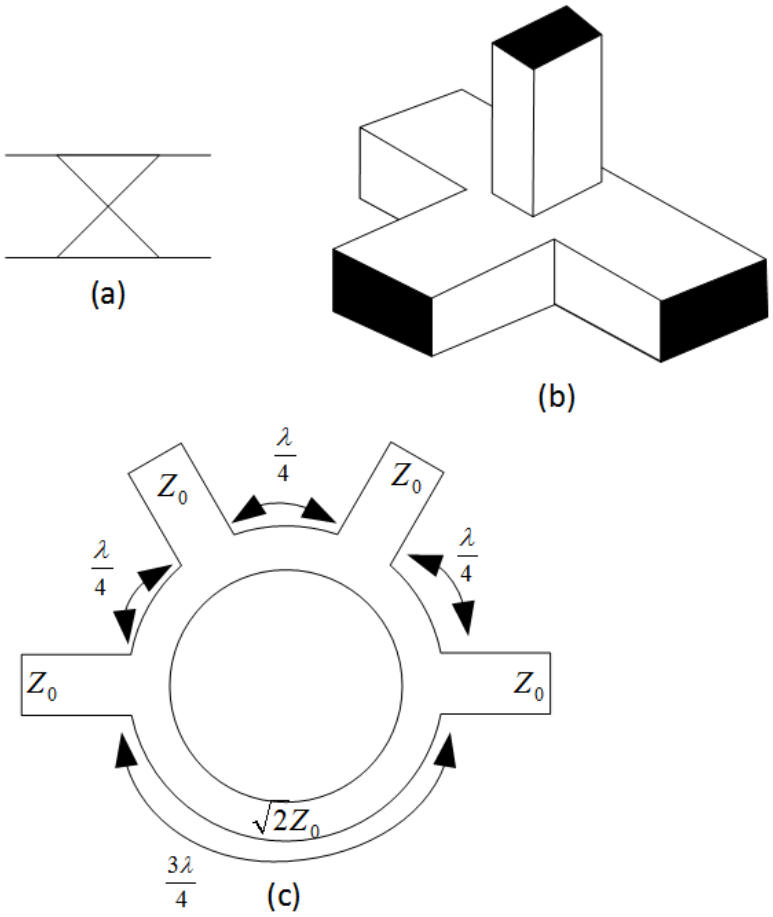

Figure 4.1: (a) System level diagram of hybrid coupler. (b) Waveguide magic tee. (c) Microstrip ratrace coupler.

4.1.2 Operation of Right-Handed Four-Port Circulator

The operation of the four-port circulator is shown pictorially in Fig. 4.2. In the diagram, the gyrator is represented as a box with its ideal scattering matrix. Port 1 is on the lefthand side and port 2 is on the righthand side.

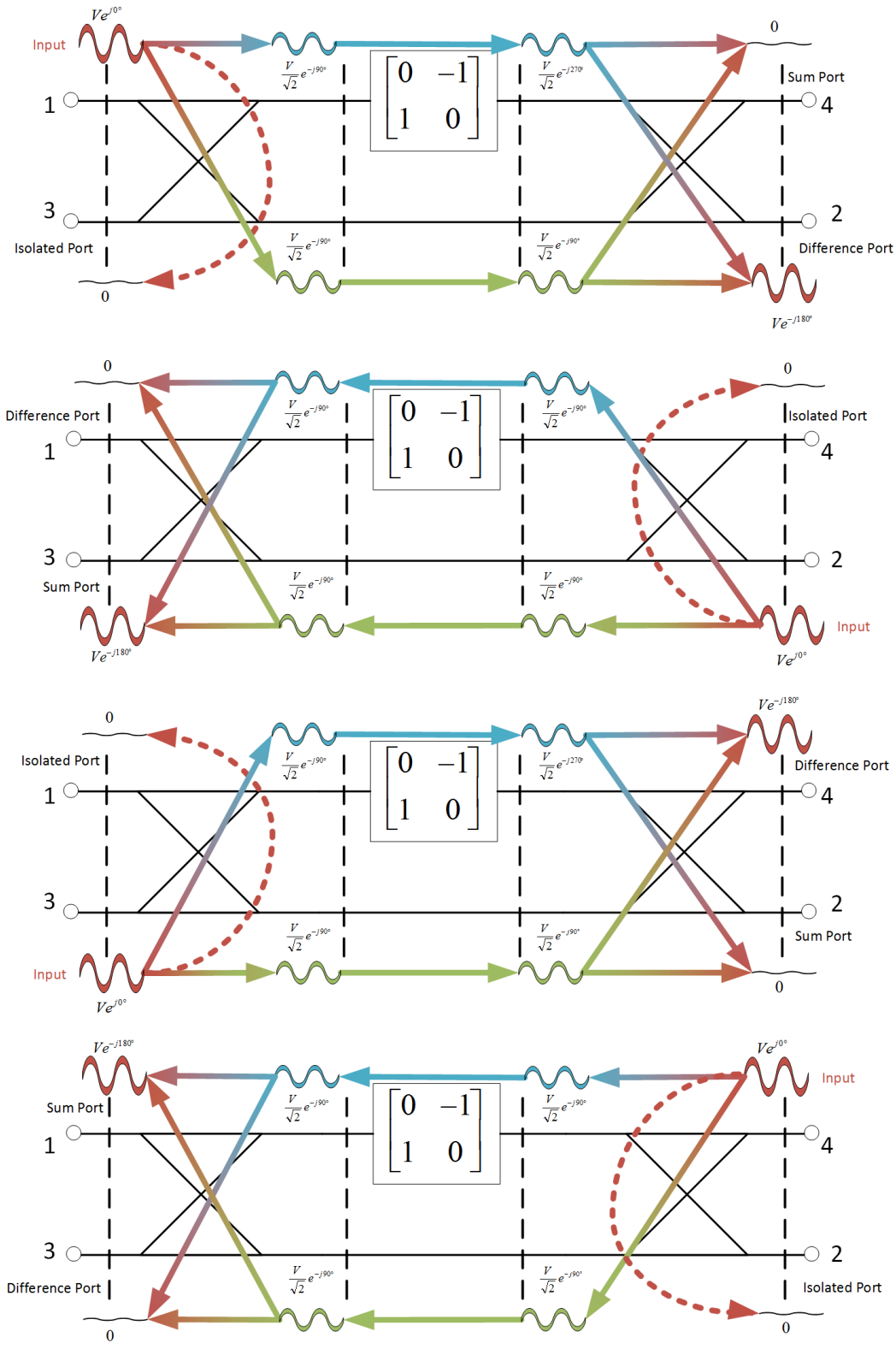

Figure 4.2: Graphical representation of operation of right-handed four-port parametric circulator. All quantities shown are in phasor form.

Consider a time-harmonic signal incident upon port 1 of the form $V_1(t) = V\cos(\omega t)$. In phasor form, this is represented as $\tilde{V}_1 = Ve^{j0^\circ}$. The lefthand hybrid (lh) evenly divides this signal between two paths: one with the gyrator and the other a short. The signal leaving the hybrid on both paths can be written in phasor form as $\frac{V}{\sqrt{2}}e^{-j90^\circ}$. The gyrator imparts a 180° phase delay on the signal passing through its path and the signal on the other path is unchanged. The righthand hybrid (rh) then acts as a combiner for two signals, one coming from the gyrator with the form $\frac{V}{\sqrt{2}}e^{-j270^\circ}$ and one from the short of the form $\frac{V}{\sqrt{2}}e^{-j90^\circ}$. Port 4 of the circulator then becomes the righthand hybrid's sum port, and the output is then $V_4(t) = 0$. Port 2 of the circulator becomes the righthand hybrid's difference port, and the output from this port is then $V_2(t) = -V\cos(\omega t)$. From this, one can infer that $S_{21} = -j$ and $S_{31} = S_{41} = 0$. One can infer the remaining S-parameters through a similar approach keeping in mind that the gyrator imparts a 180° phase shift to a signal traveling from the lefthand hybrid to the righthand hybrid, but imparts no phase shift to a signal traveling from the righthand hybrid to the lefthand hybrid. Since both hybrids are matched at all four ports and the gyrator is matched at all four ports, all four ports of the circulator will be matched as well. The four-port circulator therefore has the scattering matrix

$$S = -j\begin{pmatrix} 0 & 0 & 0 & 1 \\ 1 & 0 & 0 & 0 \\ 0 & 1 & 0 & 0 \\ 0 & 0 & 1 & 0 \end{pmatrix} \tag{4.2}$$

This is almost the ideal scattering matrix of equation 1.19 except there is an additional 90° phase shift imparted on a circulated signal. It is also worth noting that instead of 180° hybrids, a designer can also use four-port quadrature couplers (such as a branchline coupler) to achieve the four-port circulator. As an exercise to the reader, it may be shown that the matrix of equation 4.2 would become

$$S = \begin{pmatrix} 0 & 0 & 0 & 1 \\ j & 0 & 0 & 0 \\ 0 & -1 & 0 & 0 \\ 0 & 0 & j & 0 \end{pmatrix} \tag{4.3}$$

4.1.3 Reversal of Rotation Sense

One important property of the parametric gyrator is its ability to reverse its values of S_{21} and S_{12} by changing the LO phase. Recall that the choice of $\alpha = 0$ and $\beta = \frac{\pi}{2}$ in equation 3.6 yielded the scattering matrix of 3.7. By now choosing $\alpha = \frac{\pi}{2}$ and $\beta = 0$, the scattering matrix of equation 3.6 changes to

$$S = j \begin{pmatrix} 0 & 1 \\ -1 & 0 \end{pmatrix} \tag{4.4}$$

A simple analysis similar to that of the previous section can be used to show that the scattering matrix becomes

$$S = -j \begin{pmatrix} 0 & 1 & 0 & 0 \\ 0 & 0 & 1 & 0 \\ 0 & 0 & 0 & 1 \\ 1 & 0 & 0 & 0 \end{pmatrix} \tag{4.5}$$

A pictorial representation of the left-handed version of the four-port circulator is shown in Fig. 4.3. Note the only change to the topology was reversing the phase shifting direction of the gyrator. In practice, this can be accomplished trivially by using switched delay lines or phase shifters for the LO signal.

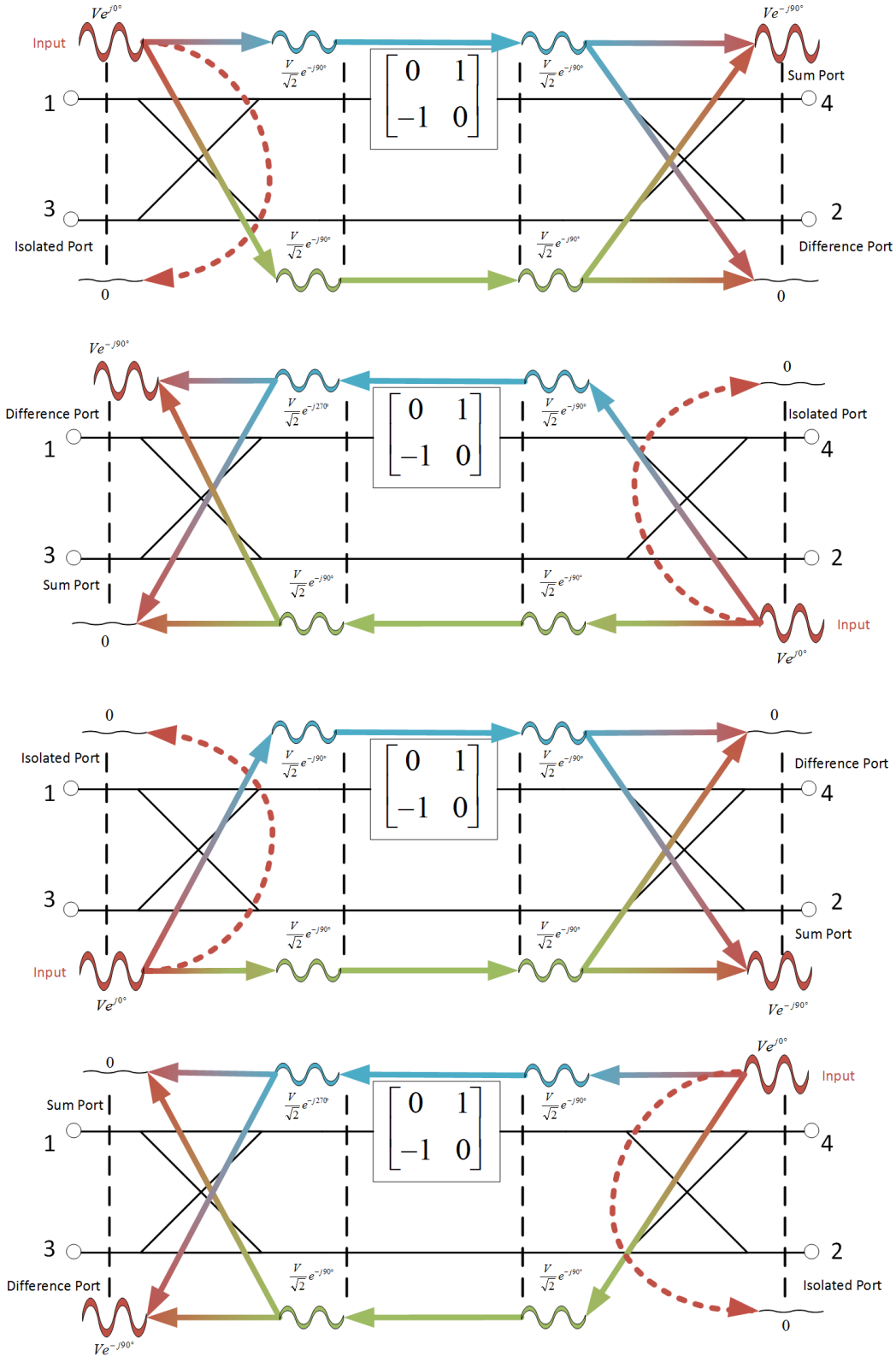

Figure 4.3: Graphical representation of operation of left-handed four-port parametric circulator.

4.2 Transmission Phase and Group Delay of Parametric Gyrator

As mentioned in the introduction to this chapter, the physical realization of the gyrator-circulator requires knowledge of the transmission properties of the gyrator. Although the amplitude response was explored in chapter 3, the phase response is also of interest. Since the ideal gyrator transmission phase must be equal to $2n\pi$ in one direction and $(2n+1)\pi$ in the other for $n \in \mathbb{R}$, it is important to be able to predict this phase in case it needs to be adjusted to satisfy these conditions. In addition, in order for the delay of the two paths connecting the hybrids in the four-port topology to be the same, it is imperative that the group delay of the gyrator be estimated as well.

4.2.1 Derivation

The impedance matrix of equation 3.10 can be utilized to predict the phase imparted by a nonlinear capacitor. The voltage gain of a two-port network with respect to its impedance parameters is

$$A_v = \frac{Z_{21}Z_L}{(Z_{11}+Z_G)(Z_{22}+Z_L) - Z_{12}Z_{21}} \tag{4.6}$$

The phase of this quantity is readily found from its real and imaginary parts.

$$\angle A_v = \arctan\left(\frac{\Im(A_v)}{\Re(A_v)}\right) \tag{4.7}$$

$\angle A_v$ can be interpreted as the phase of the signal exiting the nonlinear capacitor. In the previous sections, it was implicitly assumed that filters enforced a single frequency component at each port of the parametric modulators used to construct the gyrator. To accurately model the transmission phase, the filters must now be accounted for. The filters tuned to ω_{IF} are assumed to impart a phase delay of $\theta_{\mathrm{IF}}(\omega)$ within their passbands. The filter tuned to ω_+ is assumed to impart a phase delay of $\theta_+(\omega+\omega_{\mathrm{LO}})$ in its passband. Denoting

the transmission phase from port 1 to port 2 as $\theta_{21}(\omega)$ and that from port 2 to port 1 as $\theta_{12}(\omega)$, a new equivalent model of the gyrator is given in Fig. 4.4.

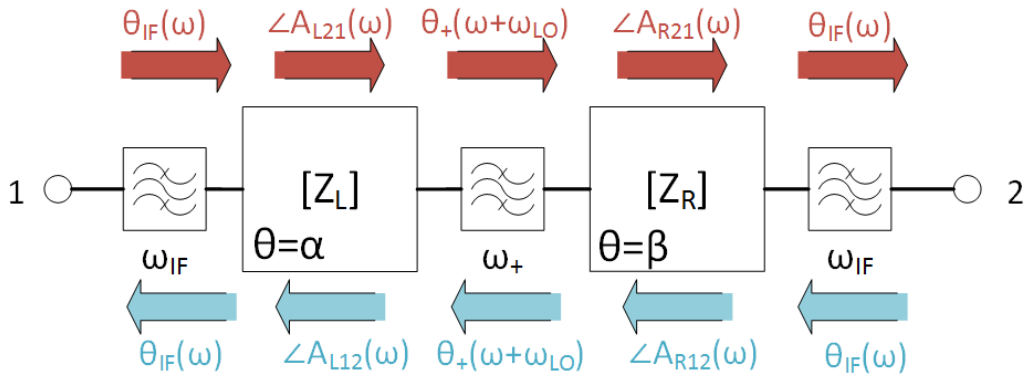

Figure 4.4: Expanded model of parametric gyrator that explicitly accounts for the effects of the necessary filters. The components Z_L and Z_R can both be described by the matrix of 3.10 by substituting the value of θ with α and β, respectively. As before, these quantities denote the LO phase.

Ignoring the effect of the loss resistance R_c in the modulators, the relevant voltage gain quantities can be computed:

$$A_{\mathrm{L21}} = e^{-j\alpha} A_{v\uparrow}(\omega) \tag{4.8a}$$

$$A_{\mathrm{L12}} = e^{j\alpha} A_{v\downarrow}(\omega) \tag{4.8b}$$

$$A_{\mathrm{R21}} = e^{-j\beta} A_{v\downarrow}(\omega) \tag{4.8c}$$

$$A_{\mathrm{R12}} = e^{j\beta} A_{v\uparrow}(\omega) \tag{4.8d}$$

The other quantities can be found from:

$$A_{v\uparrow}(\omega) = \frac{j\frac{\psi}{\omega_{\mathrm{IF}}C_0(1-\psi^2)}R}{Z_{\mathrm{IN}}Z_{\mathrm{OUT}} + \frac{\psi^2}{\omega_{\mathrm{IF}}\omega_+ C_0^2(1-\psi^2)^2}} \tag{4.9a}$$

$$A_{v\downarrow}(\omega) = \frac{j\frac{\psi}{\omega_+ C_0(1-\psi^2)}R}{Z_{\mathrm{IN}}Z_{\mathrm{OUT}} + \frac{\psi^2}{\omega_{\mathrm{IF}}\omega_+ C_0^2(1-\psi^2)^2}} \tag{4.9b}$$

$$Z_{\mathrm{IN}} = j\left(\omega_{\mathrm{IF}}L_S - \frac{1}{\omega_{\mathrm{IF}}C_0(1-\psi^2)}\right) + R \tag{4.9c}$$

$$Z_{\mathrm{OUT}} = j\left(\omega_+ L_L - \frac{1}{\omega_+ C_0(1-\psi^2)}\right) + R \tag{4.9d}$$

$$R = \frac{\psi}{\sqrt{\omega_{\mathrm{IF}}\omega_+}C_0(1-\psi^2)} \tag{4.9e}$$

The inductor values L_S and L_L are given by equations 3.12 and 3.13, respectively. Finally, the transmission phase in each direction is given by equation 4.10. For the gyrator, as before, one should select $\alpha = 0$ and $\beta = 90°$ or $\alpha = 90°$ and $\beta = 0$.

$$\theta_{21}(\omega) = 2\theta_{\mathrm{IF}}(\omega) + \angle A_{\mathrm{L21}}(\omega) + \theta_+(\omega + \omega_{\mathrm{LO}}) + \angle A_{\mathrm{R21}}(\omega) \tag{4.10a}$$

$$\theta_{12}(\omega) = 2\theta_{\mathrm{IF}}(\omega) + \angle A_{\mathrm{L12}}(\omega) + \theta_+(\omega + \omega_{\mathrm{LO}}) + \angle A_{\mathrm{R12}}(\omega) \tag{4.10b}$$

The group delay from port 1 to port 2, τ_{g21}, and that from port 2 to port 1, τ_{g12}, can be found from

$$\tau_{g21} = -\frac{d}{d\omega}\theta_{21}(\omega) \tag{4.11a}$$

$$\tau_{g12} = -\frac{d}{d\omega}\theta_{12}(\omega) \tag{4.11b}$$

It is desirable for the gyrator to add no distortion to signals passing through it, which means $\tau_{g21} = \tau_{g12} =$ const. over frequency. This is achieved when θ_{21} and θ_{12} are linear over frequency and have the same slope.

4.2.2 Design Examples

Two design examples are given here to demonstrate the use of this approach. In the first example, the method is used at the center frequency to determine the additional phase delay that must be added to the gyrator in order for its behavior to approach ideal. In the second example, the group delay of an idealized gyrator is estimated.

4.2.2.1 Example 1 - Center Frequency Transmission Phase

$$f_{\mathrm{IF}} = 500 \text{ MHz}$$

$$f_{\mathrm{LO}} = 1000 \text{ MHz}$$

$$C_0 = 1 \text{ pF}$$

$$\psi = 0.3$$

$$\theta_{\mathrm{IF}} = -100^\circ \text{ at } 500 \text{ MHz}$$

$$\theta_{+} = -150^\circ \text{ at } 1500 \text{ MHz}$$

Assuming the lefthand modulator has a LO phase of 0° and the righthand modulator has a LO phase of 90°, the analysis starts from equations 3.12 and 3.13 to find that $L_S = 111.3$ nH and $L_L = 12.4$ nH. From equation 4.9e, $R = 60.6\Omega$. These quantities can be used to find that $A_{\mathrm{L21}} = A_{\mathrm{L12}} = -90^\circ$, $A_{\mathrm{R12}} = 0^\circ$ and $A_{\mathrm{R12}} = -180^\circ$. Thus, $\theta_{21} = -620^\circ$ and $\theta_{12} = -440^\circ$. Therefore, an extra -100° of phase delay should be added to the gyrator for its S-matrix to become that of equation 4.12 at $\omega = \omega_{\mathrm{IF}}$, which is the ideal gyrator.

$$S = \begin{pmatrix} 0 & -1 \\ 1 & 0 \end{pmatrix} \tag{4.12}$$

4.2.2.2 Example 2 - Group Delay

$$f_{\mathrm{IF}} = 500 \text{ MHz}$$

$$f_{\mathrm{LO}} = 1000 \text{ MHz}$$

$$C_0 = 1 \text{ pF}$$

$$\psi = 0.3$$

$$\theta_{\mathrm{IF}} = 0^\circ$$

$$\theta_+ = 0^\circ$$

The filters are assumed to be phaseless, since any number of filters can be chosen in the event the nonlinear capacitors have undesirable phase characteristics. The values of L_L, L_S and R are the same as in Example 1. First, the value of $\theta_{21}(\omega)$ can be evaluated. The values of $\angle A_{L21}$, $\angle A_{L12}$, $\angle A_{R21}$, and $\angle A_{R12}$ are computed and shown in Fig. 4.5 along with the transducer gain normalized to the ideal Manley-Rowe value. The frequency range corresponds to the 3 dB bandwidth of 402 - 588 MHz, or 37.2%. Now, the two phase curves can be added together to find the overall transmission phase. This exercise can be repeated for $\theta_{21}(\omega)$ as well. Shown in Fig. 4.6 is the transmission phase in both directions of the gyrator. Note that the addition of filters can serve to change the shape of the phase plot if different characteristics are required. Mathematically, this confirms the derivation of equation 3.7, as in Fig. 4.6, it is seen that the values of the transmission phase at the center frequency, 500 MHz, are exactly as predicted by 3.7. Now, the group delay is found by taking the derivative of each phase curve with respect to frequency. The phase slope is found to be 0.8801 °/MHz through a line of best fit ($R^2 = 0.9987$), meaning the group delay is 2.44 ns. If more realistic filters were included, the total group delay of the gyrator would be this calculated value plus the group delay of each individual filter.

4.3 Adjusted Circulator Topologies

Shown in Fig. 4.7 are two topologies that can be used to physically realize the gyrator-circulator. Figure 4.7a shows the familiar four-port circulator. Two new elements have been added: a delay balancer and a phase compensator. The phase compensation is used to ensure the gyrator provides a $2n\pi$ phase

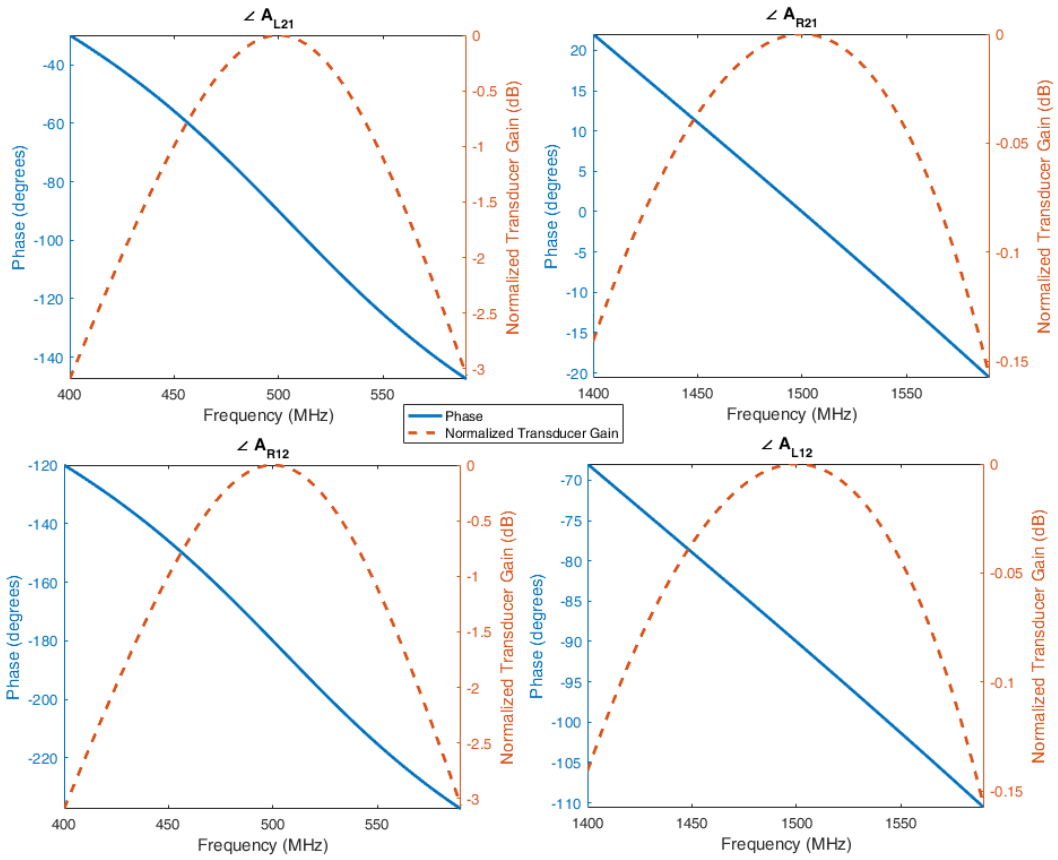

Figure 4.5: Computed values of $\angle A_{L21}$, $\angle A_{L12}$, $\angle A_{R21}$, and $\angle A_{R12}$ alongside modulator/demodulator transducer gain. The gain is normalized to the ideal Manley-Rowe value: $\frac{f_p+f}{f}$ for an upconverter and $\frac{f}{f+f_p}$ for a downconverter.

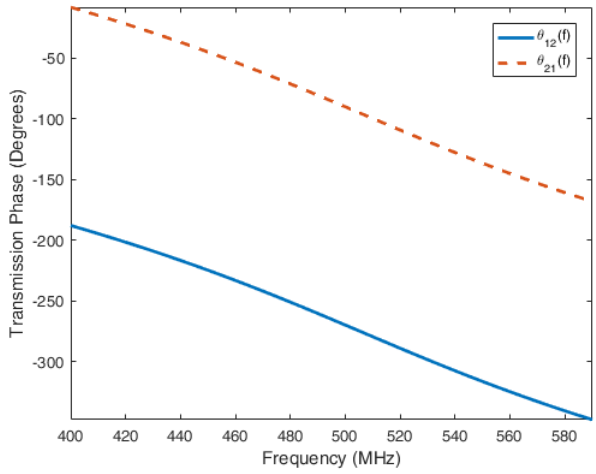

Figure 4.6: Transmission phase characteristic in each direction over the 3 dB bandwidth of the gyrator.

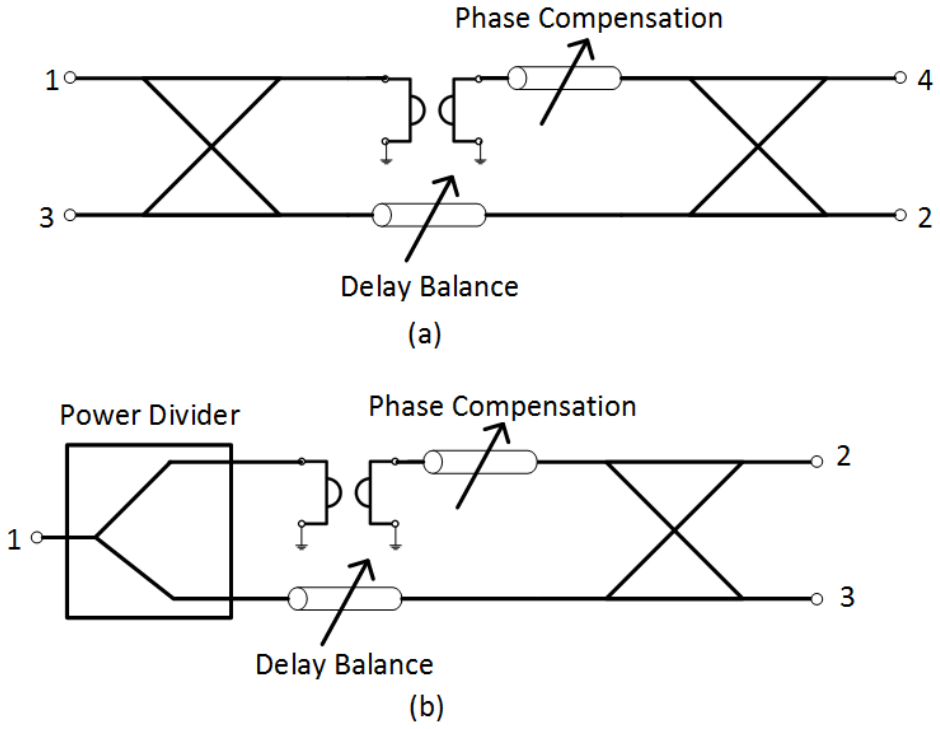

Figure 4.7: (a) Adjusted four-port circulator topology and (b) approximation of three-port circulator. The phase compensation can be used to tune the center frequency of the gyrator to the center frequency of the hybrids and dividers. The delay balance has a time delay equal to the combined delay of the gyrator and the phase compensation.

shift in one direction and a $(2n+1)\pi$ phase shift in the other at the center frequency of operation. This is necessary to ensure the gyrator operates at the same center frequency of the two hybrids in order to ensure proper operation. In the arm below the gyrator, the delay balancer is adjusted to provide a path delay equal to the delay of both the gyrator and the phase compensator. Its group delay should be the same as in expression 4.11. Figure 4.7b shows an approximation to the three-port circulator that can be referred to as a *quasi-circulator*. The quasi-circulator uses just one hybrid, as well as an in-phase power divider. The power divider's matrix can be expressed as

$$S_{\text{Power Divider}} = \frac{-j}{\sqrt{2}} \begin{pmatrix} 0 & 1 & 1 \\ 1 & 0 & 0 \\ 1 & 0 & 0 \end{pmatrix} \tag{4.13}$$

This divider can be realized in different ways, such as a Wilkinson divider. The choice of the term *quasi-circulator* is evident from the S-parameters of the three-port circulator approximation, shown in

$$S = \begin{pmatrix} 0 & 0 & -1 \\ 1 & 0 & 0 \\ 0 & 0 & 0 \end{pmatrix} \tag{4.14}$$

Ports 2 and 3 are isolated from each other, meaning no signal can travel between them irrespective of direction of propagation. This isolation is controlled by the isolation of the hybrid, meaning even if the gyrator provides poor circulator performance, a well-designed hybrid can compensate for it if a designer only wishes to deeply isolate one port pair. An example of when this is useful is in the full-duplex transceiver. A representation of the use of the quasi-circulator in the full-duplex transceiver is shown in Fig. 4.8. Since it is desired that no signal ever travel between the transmitter and the receiver, full circulator operation is not necessary.

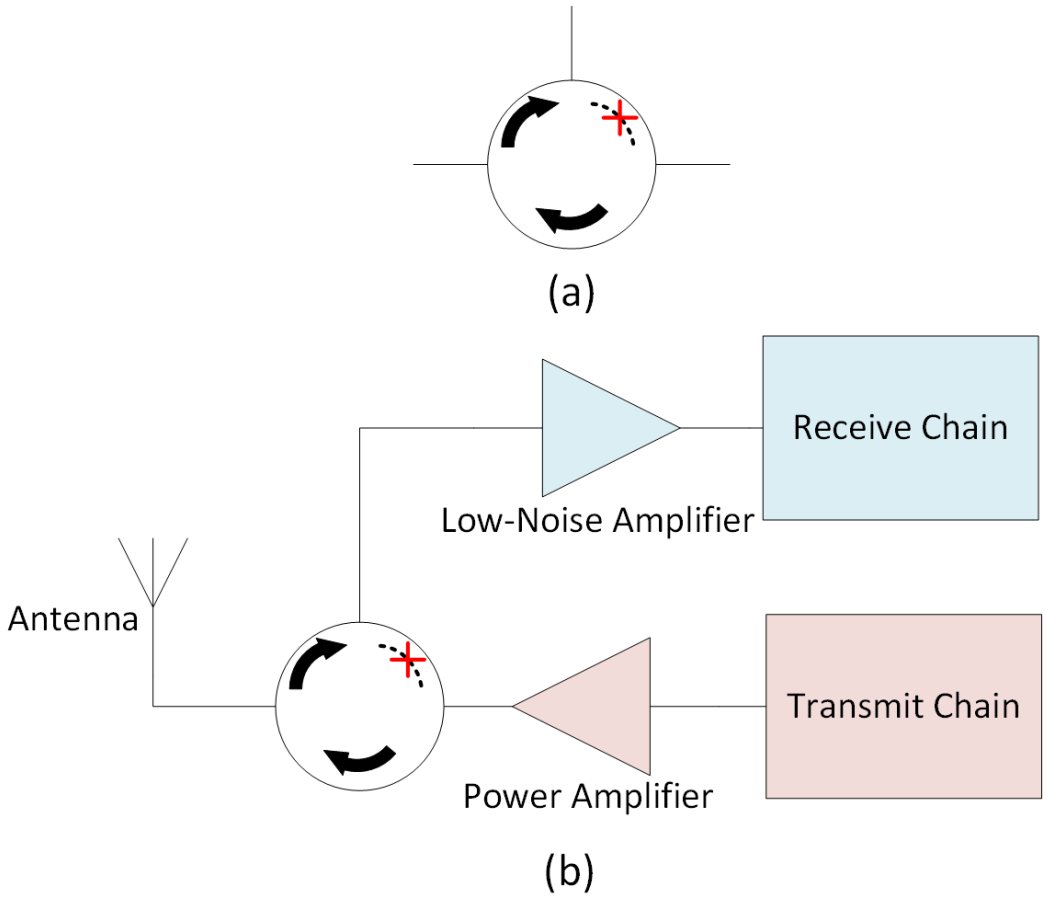

Figure 4.8: (a) Symbol for a quasi-circulator. (b) Full-duplex communication system with quasi-circulator.

4.4 Bandwidth Performance

The circulator isolation bandwidth is controlled by both the bandwidths of the hybrids as well as the amplitude bandwidth of the gyrator. Even if the gyrator's bandwidth is quite broad, the hybrids have limitations based on their topology. It is of interest, then, to investigate the upper limits on bandwidth due to the hybrids themselves.

4.4.1 Ideal Four-Port Gyrator-Circulator Isolation Performance

S-parameter simulations were performed to estimate the maximum achievable bandwidth of the gyrator-circulator using ideal, lossless transmission lines to create various hybrid coupler topologies. The gyrator was modeled as a two-port network with its S-parameters being that of 1.22 over all frequencies. Since this circulator is ideal, it provides infinite isolation at the center of its band, but this isolation rolls off with frequency. The isolation bandwidth of the gyrator-circulator is defined to be the fractional bandwidth over which the circulator provides at least 20 dB of isolation.

4.4.1.1 Ratrace Hybrid

The ratrace coupler, a 180° hybrid shown in Fig. 4.1, provides a maximum achievable isolation bandwidth of 17.1%, as seen in Fig. 4.9.

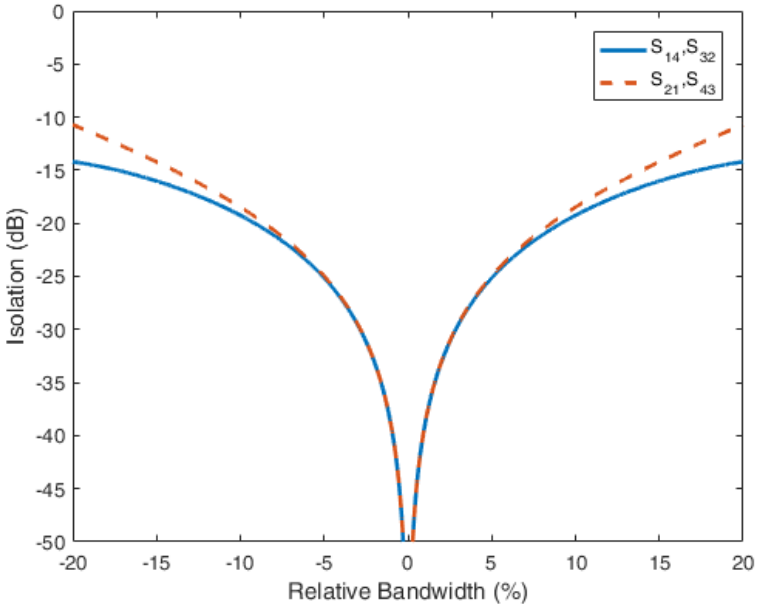

Figure 4.9: Isolation performance of idealized four-port circulator using ratrace hybrids. The isolation characteristic is not identical between all port pairs.

4.4.1.2 Branchline Hybrid

The branchline coupler is a quadrature coupler shown schematically in Fig. 4.10. Since it is also a four-port device like the 180° hybrid, it is connected in the same fashion as the 180° hybrid in the topologies of 4.7. Observing the S-parameter simulation in Fig. 4.11, it displays even less symmetry than the ratrace hybrid, but the bandwidth of the narrower curve is 17.6%, which is more or less the same as the circulator constructed with ratrace hybrids.

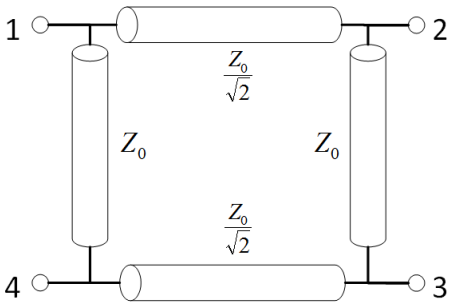

Figure 4.10: Transmission line realization of branchline coupler. All lines are 90° in electrical length.

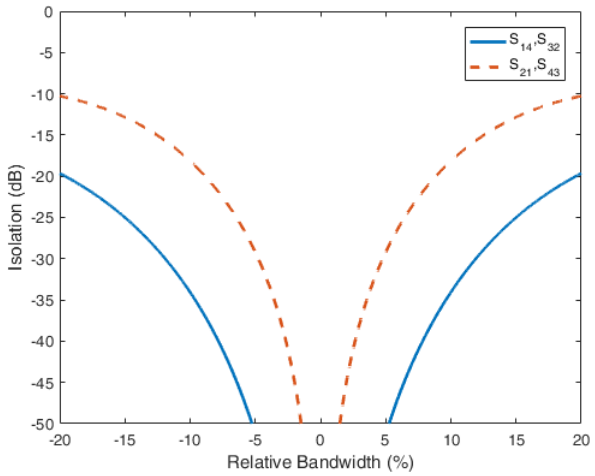

Figure 4.11: Isolation performance of idealized four-port circulator using branchline hybrids. The isolation characteristic is not identical between all port pairs.

4.4.2 Broadband Realization of the Gyrator-Circulator

In order to create a broadband architecture for the gyrator-circulator, a designer must broaden the bandwidths of both the hybrids and the gyrator itself. Although there are many topologies of hybrids that can achieve this, this section focuses on the multistage branchline hybrid as an example. Although there have been several efforts in broadbanding the branchline coupler, one simple topology called the double-box branchline [19] can be employed here. A schematic representation of the idealized gyrator-circulator with with the double-box hybrids is shown in Fig. 4.12. S-parameter simulations, shown

in Fig. 4.13, demonstrate a 20 dB isolation bandwidth of 30.6%, which is 1.7 times the bandwidth achievable by a single-stage branchline coupler.

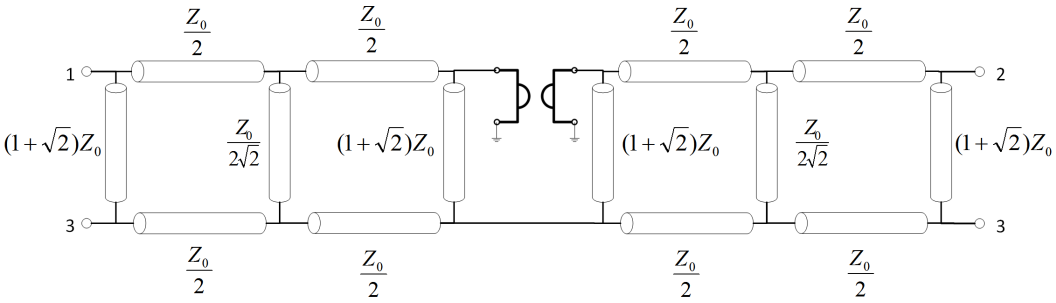

Figure 4.12: Topology of the broadbanded circulator. All transmission lines are 90° in electrical length.

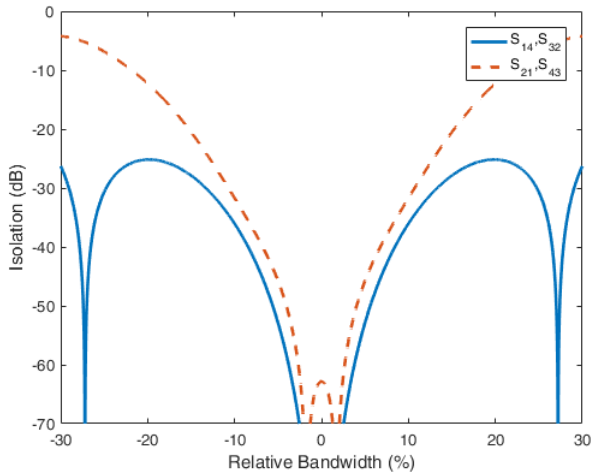

Figure 4.13: Isolation performance of idealized four-port circulator. The isolation characteristic is not identical between all port pairs.

4.5 Design Example

A four-port parametric circulator is to be designed for operation at 500 MHz. The gyrator used in the circulator should be designed with a noise figure less than 3.4 dB. The circulator should be matched to a system impedance of 50 Ω. The parametric gyrator is to be constructed from a variable capacitance that has the following properties:

$$C_0 = 1 \text{ pF}$$

$$\psi = 0 - 0.45$$

$$R_c = 2.5\ \Omega$$

The design begins by selecting an appropriate LO frequency ω_{LO} and modulation parameter ψ. Since a large modulation parameter yields a lower noise factor, the highest possible modulation parameter ($\psi = 0.45$) is used to find the lowest possible LO frequency. Using equation 3.33, the noise figure can be plotted for various LO frequencies as in Fig. 4.14.

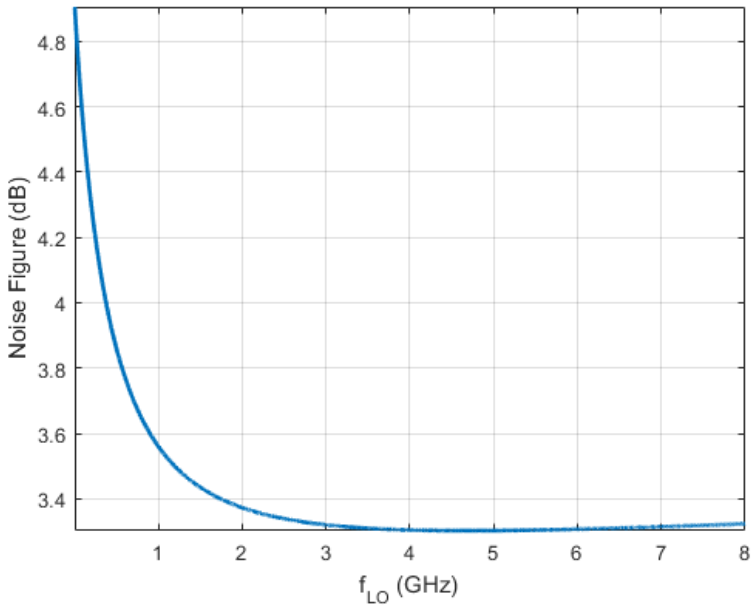

Figure 4.14: Noise figure of the gyrator for various LO frequencies. The dynamic quality factor Q_{d} is approximately 160 for the highest supported modulation parameter.

Choosing f_{LO} to be 2 GHz gives a slight margin below 3.4 dB noise figure. Now, the actual modulation parameter can be selected. Since $R_c = 2.5\ \Omega$ and $\omega_{\text{LO}} = 2\pi \times 2$ GHz, equation 3.18 can be used to find that ψ must be 0.41 to match to 50 Ω. This is close to the maximum modulation parameter, and thus yields an actual noise figure of the gyrator still in the vicinity of 3.4 dB. From equations 3.12 and 3.13, the tuning inductances are $L_S = 152.3$ nH and $L_L = 6.1$ nH. From equation 3.19, $Q_{\text{d}} = 153$ and from equation 3.21,

$\xi^2 = 0.00127$. Finally, from equation 3.25, the predicted insertion loss of the gyrator is 0.61 dB. Before simulating the gyrator, a simple S-parameter simulation using ratrace couplers created with ideal transmission lines can be used to predict the isolation at the center frequency for varying levels of gyrator insertion loss. Observing such a simulation in Fig. 4.15, it can be estimated that this gyrator in a four-port circulator with ideal ratrace couplers will provide a center frequency isolation of 29.4 dB.

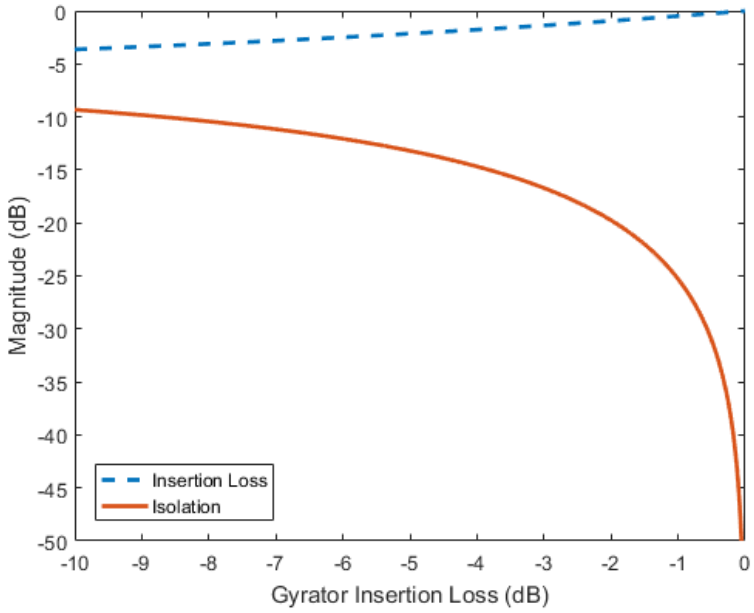

Figure 4.15: Four-port circulator insertion loss and isolation between port pairs for increasing levels of gyrator insertion loss.

The gyrator was then simulated using a harmonic balance routine. The three filters used were Bessel-Thompson filters, chosen because of their highly linear phase response. The two ω_{IF} filters had a center frequency of 500 MHz with 10% fractional bandwidth. The ω_+ filter had a center frequency of 2500 MHz with a bandwidth of 10%, though a narrower bandwidth could have been tolerated. The simulation was performed in Keysight ADS using the schematic shown in Fig. 4.16. The tuning inductances were adjusted slightly, as the filters provide some reactance even at the center frequency that changes the tuning requirements.

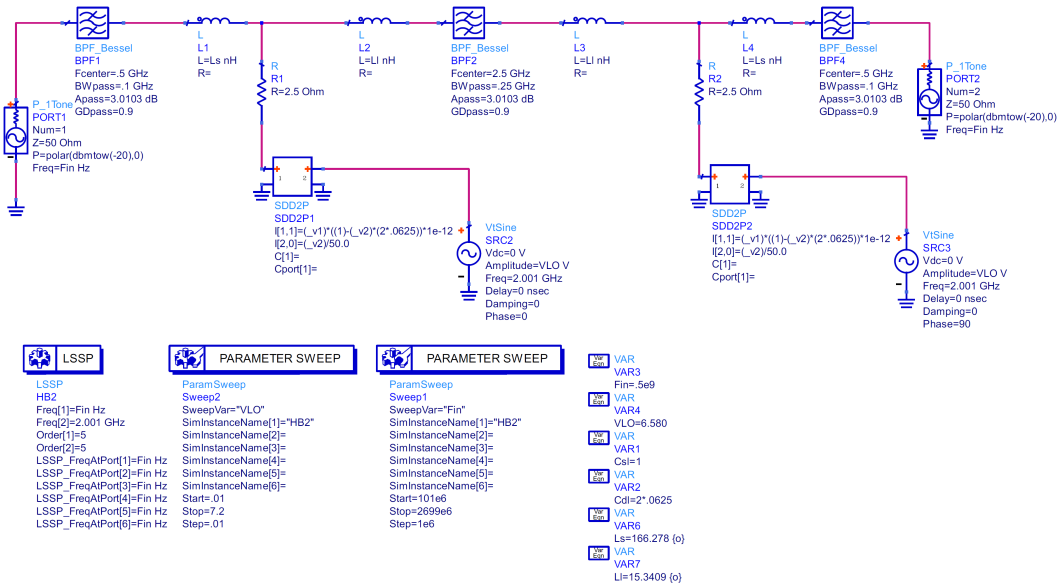

Figure 4.16: Keysight ADS simulation of gyrator. LSSP simulation performs the function of a typical harmonic balance simulation, but makes computation of quantities like insertion loss and transducer gain simpler, especially when the frequency is swept over some range.

After setting up the simulation, the modulation parameter was swept over the supported range of the nonlinear capacitor. As seen in Fig. 4.17, the optimal value of ψ was in the vicinity of the predicted value of 0.41. The insertion loss for this was slightly better than predicted, at about 0.55 dB. With the gyrator optimized, a simulation was performed over frequency as shown in Fig. 4.18. It can be seen that the gyrator's amplitude response is centered about 504 MHz with a 3 dB bandwidth of 6.3%. The phase of S_{21} and S_{12} at 500 MHz is -348° and -528°, respectively, meaning an additional 12° of phase delay is necessary to operate the gyrator as a circulator at 500 MHz. The transmission phase is quite linear, and can be approximated with equation 4.15 where f is the frequency in MHz.

$$\theta_{12} \approx -7.56f + 3253 \tag{4.15}$$

Of course, this approximation is only valid within the 3 dB bandwidth. Since the phase slope is 7.56 °/MHz, from equation 4.11, it is expected that this gyrator will have a group delay of about 21 ns. The delay balance should be about this amount, keeping in mind the additional 12° phase compensation

will affect the group delay a bit.

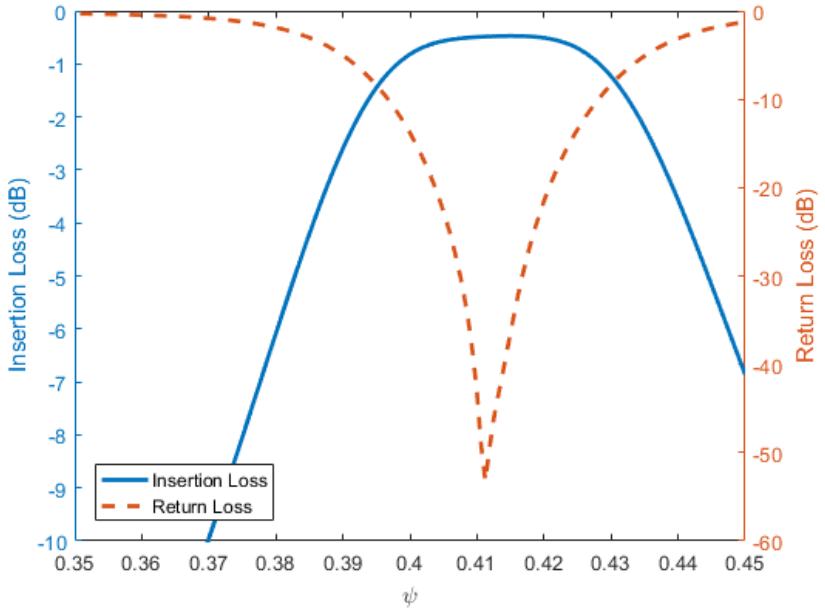

Figure 4.17: Simulation of gyrator insertion loss (magnitude of S_{21}, S_{12}) and return loss (magnitude of S_{11}, S_{22}) for varying ψ.

The four-port gyrator-circulator was then simulated in Keysight ADS. The additional 12° phase delay was accomplished by placing an ideal transmission line inline with the gyrator. The delay balancer is also an ideal transmission line. The couplers used were branchline couplers. Although these are quadrature couplers, the performance should not differ drastically from a four-port gyrator-circulator using 180° hybrids. Simulation results are displayed in Fig. 4.19 and the ADS setup is shown in Fig. 4.20. Although the performance of only one port pair is displayed here, the reader is encouraged to duplicate the simulation setup to observe the circulator's performance in more detail. The 20 dB isolation bandwidth is 6.2%, which is almost the same as the gyrator's 3 dB amplitude bandwidth. The isolation at midband is 29.55 dB, which is in good agreement with the prediction.

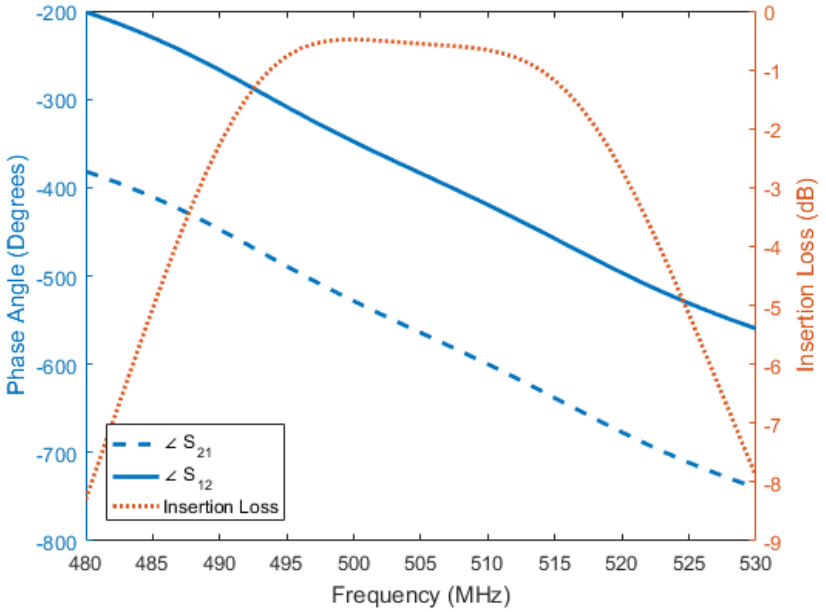

Figure 4.18: Simulation of gyrator insertion loss and transmission phase over frequency.

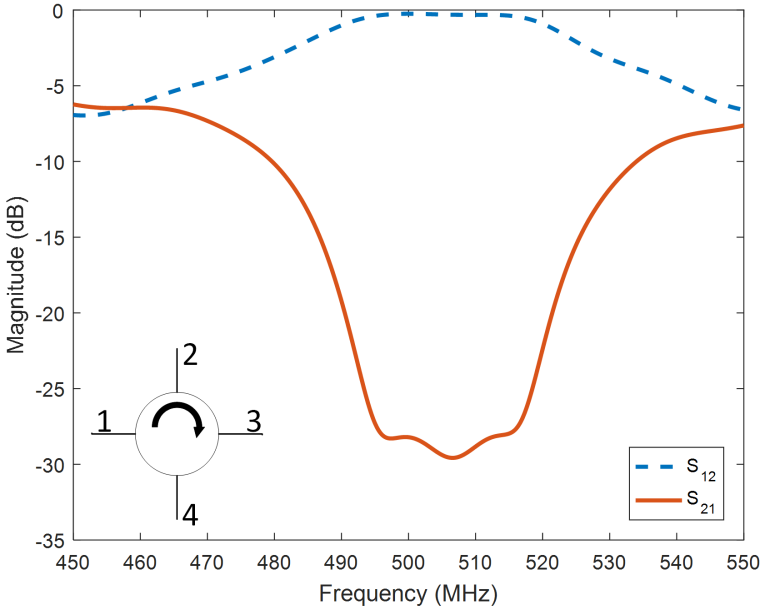

Figure 4.19: Magnitude of S_{21} and S_{12} of the gyrator-circulator.

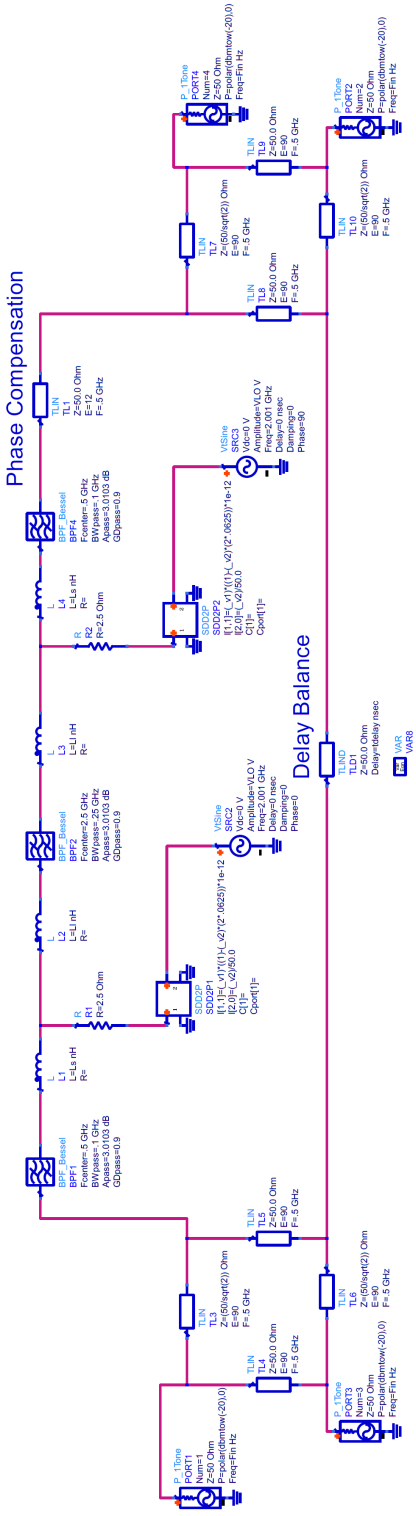

Figure 4.20: Keysight ADS simulation schematic for four-port parametric circulator.

CHAPTER 5

CONCLUSION

5.1 Findings of this Work

This work has verified the findings of Kamal [12] and performed a more in-depth analysis of the parametric gyrator and its relation to the four-port circulator and three-port quasi-circulator. This gyrator topology has a very wide design space, and it is still quite unexplored. There have been both older and modern attempts to create parametric circulators [20, 21, 22], but none have achieved any more than 5% bandwidth. Even the design example under idealized conditions in this work only achieved 6.2% bandwidth, but the potential of this circulator topology for much higher bandwidths is very enticing, even though the design space still requires exploration. This parametric gyrator has a fair share of disadvantages as well. Its performance sensitivity to losses in the filters and nonlinear capacitors is probably its greatest weakness. Its advantages include the need for only two nonlinear capacitors modulated at two different LO phases (compared to the three used in [21] with three different LO phases); the differential phase shift is independent of frequency, which offers the potential for extreme broadbanding; and its fairly simple design.

5.2 Areas of Future Research

Several avenues of future research in this device topology have been considered by the author.

5.2.1 Gyrator Loss Compensation

One major disadvantage of the parametric gyrator is the need for low-loss filters and low-loss varactors in order to implement the device, meaning the insertion loss of the gyrator is likely a major issue. One possible remedy for this is the use of *four-frequency parametric devices*. Several researchers [23, 24, 25] have found that a hybrid parametric converter that utilizes both the non-inverting and inverting mode at the same time can exhibit a gain higher than the Manley-Rowe limit of $\frac{f_+}{f_{\text{IF}}}$ while still maintaining a positive input resistance. Use of such a device could be used to overcome filter losses, or even create a gyrator with insertion gain. It is unknown to the author at this time if such a device is practical or if the noise figure of such a device would be considerably better or worse. Intuitively, the author believes the noise figure would be higher, as the four-frequency devices make use of *idler* terminations that can be resistive in nature, and this resistance can really only serve to add noise to the system. Perhaps this can be acceptable if a circulator with gain is constructed, as it could function as a low-noise amplifier for the receiver system, and so a higher noise figure could be tolerated, since the circulator-amplifier combination could have lower noise figure than a separate circulator and amplifier system.

5.2.2 Gyrator with Large Tuning Range

In practice, parametric converters are often subject to narrow bandwidth. Since the differential phase shift afforded by the gyrator is independent of frequency, the gyrator could potentially have a large tuning range, which could be accomplished with a variable phase shifter inline with the the gyrator itself. At this time, a suitable topology for the parametric gyrator that could realize this tuning feature without significantly affecting the insertion loss is unknown to the author.

5.2.3 Broadening the Amplitude Bandwidth of Parametric Gyrator

As one can imagine, the use of a simple tuning inductance as the matching element in the parametric converters limits the bandwidth of the gyrator. In order to utilize the broadbanding techniques mentioned in chapter 4, it is imperative that the gyrator's amplitude bandwidth be as broad as, if not broader than, that of the hybrids to which it is connected. The author has explored some literature that discusses the use of multiple tuning circuits rather than just the inductance, but most promising is the theoretical work by E. S. Kuh [26]. Experimental validation of a gyrator with more than 30% bandwidth is necessary to eventually achieve a circulator with at least that amount of bandwidth.

5.3 Concluding Remarks

One day, a broadband circulator could be realized using the principles discussed here. At high frequencies where the hybrid couplers are physically small, this type of circulator could prove advantageous in communication systems, especially if it could be used also as an amplification device. Since the parametric circulator uses a sinusoidal LO signal to operate, it could easily make use of the LO already present for mixing stages in communication systems. Of course, more analysis is required to determine whether this circulator is suitable for a communication system. It seems possible to design a gyrator with linear phase over its 3 dB bandwidth, but experimental validation is necessary to characterize the actual harmonic distortion properties of the gyrator. Perhaps this document will be an inspiration to a future researcher to answer these questions, just as the work of A. K. Kamal was an inspiration to this author.

REFERENCES

[1] M. Faraday, "On a peculiar class of acoustical figures; and on certain forms assumed by a group of particles upon vibrating elastic surfaces," in *Phil. Trans. R. Soc. Lond.*, vol. 121, Jan. 1831, pp. 299–340.

[2] G. F. FitzGerald, "On the driving of electromagnetic vibrations by electro-magnetic and electrostatic engines," *The Electrician*, vol. 28, pp. 329–330, Jan 1892.

[3] J. P. Gittins, J. C. Vokes, and C. S. Whitehead, "A broadband parametric amplifier," *International Journal of Electronics*, vol. 24, no. 4, pp. 333–351, 1968. [Online]. Available: http://dx.doi.org/10.1080/00207216808938029

[4] M. Uenohara and J. P. Elward, "Parametric amplifiers for high sensitivity receivers," *IEEE Transactions on Military Electronics*, vol. 8, no. 3, pp. 273–281, July 1964.

[5] M. Uenohara, M. Chruney, K. M. Eisele, D. C. Hanson, and A. L. Stillwell, "4-gc parametric amplifier for satellite communication ground station receiver," *The Bell System Technical Journal*, vol. 42, no. 4, pp. 1887–1908, July 1963.

[6] K. P. Grabowski, "A nondegenerate traveling-wave parametric amplifier," *IRE Transactions on Microwave Theory and Techniques*, vol. 10, no. 2, pp. 103–107, March 1962.

[7] P. Meerholz, "Radar sensitivity with degenerate parametric amplifier front end," *Proceedings of the IEEE*, vol. 51, no. 7, pp. 1043–1043, July 1963.

[8] R. Adler and W. S. V. Slyck, "The electron beam parametric amplifier as a radar system component," *IRE Transactions on Military Electronics*, vol. MIL-5, no. 2, pp. 66–71, April 1961.

[9] T. Mimura, "The early history of the high electron mobility transistor (hemt)," *IEEE Transactions on Microwave Theory and Techniques*, vol. 50, no. 3, pp. 780–782, Mar 2002.

[10] D. Pozar, Ed., *Microwave Engineering*. New York: Wiley, 2012.

[11] B. D. H. Tellegen, "The gyrator, a new electric network element," *Phillips Res. Rep.*, vol. 3, pp. 81–101, 1948.

[12] A. K. Kamal, "A parametric device as a nonreciprocal element," *Proceedings of the IRE*, vol. 48, no. 8, pp. 1424–1430, Aug 1960.

[13] J. M. Manley and H. E. Rowe, "Some general properties of nonlinear elements-part i. general energy relations," *Proceedings of the IRE*, vol. 44, no. 7, pp. 904–913, July 1956.

[14] H. E. Rowe, "Some general properties of nonlinear elements. ii. small signal theory," *Proceedings of the IRE*, vol. 46, no. 5, pp. 850–860, May 1958.

[15] J. Hamasaki, "A theory of a unilateral parametric amplifier using two diodes," *The Bell System Technical Journal*, vol. 43, no. 3, pp. 1123–1147, May 1964.

[16] M. P. Beddoes and W. D. Little, "Unilateral parametric frequency converters with nonlinear conductance and capacitance," *Proceedings of the IEEE*, vol. 52, no. 3, pp. 332–332, March 1964.

[17] R. Maurer and K. H. Locherer, "Low-noise nonreciprocal parametric amplifier with power matching at the input and output," *Proceedings of the IEEE*, vol. 51, no. 11, pp. 1589–1598, Nov 1963.

[18] K. Kurokawa and M. Uenohara, "Minimum noise figure of the variable-capacitance amplifier," *The Bell System Technical Journal*, vol. 40, no. 3, pp. 695–722, May 1961.

[19] Unknown, "Double-box branchlines," 2006. [Online]. Available: https://www.microwaves101.com/encyclopedias/double-box-branchlines

[20] A. Korpel and P. Desmares, "Experiments with nonreciprocal parametric devices," *Proceedings of the IRE*, vol. 49, no. 10, pp. 1568–1588, Oct 1961.

[21] N. A. Estep, D. L. Sounas, J. Soric, and A. Alu, "Magnetic-free non-reciprocity and isolation based on parametrically modulated coupled-resonator loops," *Nat Phys*, vol. 10, no. 12, pp. 923–927, Dec 2014, letter. [Online]. Available: http://dx.doi.org/10.1038/nphys3134

[22] N. Reiskarimian and H. Krishnaswamy, "Magnetic-free non-reciprocity based on staggered commutation," *Nature Communications*, vol. 7, pp. 11 217 EP –, Apr 2016, article. [Online]. Available: http://dx.doi.org/10.1038/ncomms11217

[23] D. K. Adams, "Analysis of four-frequency nonlinear reactance circuits," *IRE Transactions on Microwave Theory and Techniques*, vol. 8, no. 3, pp. 274–283, May 1960.

[24] E. W. Matthews, J. A. Luksch, and G. A. VerWys, "Design and operation of four-frequency parametric up-converters," *IRE Transactions on Microwave Theory and Techniques*, vol. 9, no. 1, pp. 44–52, January 1961.

[25] A. Korpel and V. Ramaswamy, "Input conductance of a four-frequency parametric up-converter," *IEEE Transactions on Microwave Theory and Techniques*, vol. 13, no. 1, pp. 96–106, Jan 1965.

[26] E. S. Kuh, "Theory and design of wide-band parametric converters," *Proceedings of the IRE*, vol. 50, no. 1, pp. 31–38, Jan 1962.